*Manuscript
Click here to view linked References

A comprehensive assessment of new absorber-exchanger designs for hybrid PVT-water collectors

María Herrando[1,2,*], Alba Ramos[1,3], Ignacio Zabalza[2], Christos N. Markides[1]

[1] *Clean Energy Processes (CEP) Laboratory, Department of Chemical Engineering, Imperial College London, London, UK*

[2] *School of Engineering and Architecture, University of Zaragoza, Zaragoza, Spain*

[3] *Solar Energy Institute, Technical University of Madrid, Spain*

* Corresponding author: mherrando@unizar.es

Abstract

In this paper, a number of new absorber-exchanger designs for hybrid PV-thermal (PVT) solar collectors are proposed, whose performance is assessed and compared from a technoeconomic perspective. The configurations involve new geometrical design features based on a flat-box structure manufactured from suitable polymeric materials, with the aim of maintaining or even improving heat transfer and overall (thermal and electrical) performance while achieving significant reductions in the overall weight and cost of the collectors. Firstly, a range of alternative sheet-and-tube (S&T) and flat-box design variations and materials for the absorber-exchanger component are considered that have the potential to meet the aforementioned aims. Selected designs (plus a benchmark reference case based on a commercially-available S&T PVT collector) are then integrated within the same PVT collector in order to compare their respective performance. Following the detailed high-level definition of these designs, these are modelled in the 3-D finite-element and multiphysics (FEM and CFD) software environment COMSOL. The specific objectives of this exercise are to: i) assess the heat transfer performance of the selected absorber-exchanger designs, ii) obtain characteristic curves that describe the steady-state thermal performance of the PVT collectors in each case, iii) estimate the thermal expansion that the PVT collector suffers and the associated thermal strains for the most promising absorber-exchanger designs, and verify that the stresses are below materials' limits, and iv) compare technoeconomically the alternatives with the reference case collector for the case of Spain. The results show that, in general, the flat-box absorber-exchanger designs are not sensitive to the flow-channel size or construction material, at least within the range of investigation. A PVT collector featuring a polycarbonate (PC) flat-box design with 3×2 mm rectangular channels appears to be a particularly promising alternative to commercial PVT collectors, achieving a slight improvement in thermal performance compared to the reference case (with a 4% higher optical efficiency and 15% lower linear heat-loss coefficient), while also lowering the weight (by around 9%) and investment cost (by about 21%) of the collector. The structural analysis shows that the maximum von Mises stress experienced in the absorber-exchanger of the PC flat-box collector is <13% of the material's yield stress (*vs*. 64% in the copper S&T collector), which is attributed to the larger thermal expansion of the PC absorber-exchanger, that leads to lower stresses. Furthermore, the maximum von Mises stress in the copper S&T collector occurs in the bonding between the pipes and the absorber plate, while this bonding is avoided in the flat-box design. Therefore, the proposed PC flat-box design is not expected to suffer higher strains than the commercially available PVT collectors.

Keywords:

absorber-exchanger, cost savings, efficiency, hybrid PVT collector, solar energy, structural analysis

Nomenclature

Abbreviations

AAD	Average Absolute Deviation
CFD	Computational Fluid Dynamics
DHW	Domestic Hot Water
FEM	Finite Element Method
hBN	Hexagonal Boron Nitride
IEA	International Energy Agency
NBL	Number of Boundary Layers
PA	Polyamide
PC	Polycarbonate
PA90	Polyamide (grade) Zytel® RS LC3090 NC010
PA30	Polyamide (grade) Zytel® RS LC3030 NC010
PBT	Payback Time
PV	Photovoltaic
PVT	(Hybrid solar) PV and Thermal collector
PVT-w	(Hybrid solar) PVT-water collector
R&D	Research & Development
ST	Solar Thermal
UTS	Ultimate Tensile Stress

Symbols

a_1	Linear heat-loss coefficient (-)
a_2	Quadratic heat-loss coefficient (-)
A_c	PVT collector aperture area (m²)
A_p	Riser pipe/channel transversal area (m²)
B	Total PVT collector width (m)
C_{bond}	Bond Conductance (W/m K)
c_p	Specific heat capacity (J/kg K)
C_0	Investment costs (€)
D	External diameter of the riser tubes (m)
D_i	Inner tube diameter (m)
D_h	Hydraulic diameter (m)
F	Standard fin efficiency (-)
F'	Collector efficiency factor (-)
F_R	Heat removal factor (-)
g	Acceleration due to gravity (m/s²)
h	Convective heat transfer coefficient (W/m² K)
H_b	Flat-box channel height (m)
I	Solar irradiance per meter square (W/m²)
k	Thermal conductivity (W/m K)
K	Incidence angle modifier of solar radiation (-)
L	Total length of the riser pipe/channel (m)
$\dot{m}_c$	Water mass flow-rate through the collector (kg/s)
$\dot{m}_{tube}$	Water mass flow-rate through the collector riser tubes (kg/s)
n	Number of riser tubes (-)
Nu	Nusselt number (-)
p	Perimeter of the riser pipes/channels (m)
Pr	Prandtl number (-)
q	Heat flow per meter square (W/m²)
R_b	Ratio of tilted to horizontal surface beam radiation (-)
Ra	Rayleigh number (-)
Re	Reynolds number (-)
S	Absorbed solar irradiance per meter square (W/m²)
T	Temperature (K)
U	Heat transfer coefficient (W/m² K)
U_L	Overall heat-loss coefficient (W/m² K)
v_w	Bulk flow speed of water through the pipe (m/s)
v_{wind}	Wind speed (m/s)
w_e	Electrical power output of the PV module (W/m²)
W	Unit fin width (m)
W_b	Flat-box channel width (m)

Greek

α_{PV}	Solar absorption coefficient of the PV module (-)
β	PVT collector tilt angle (°)
β_0	Temperature coefficient for the PV module (1/K)
β_{arg}	Volumetric expansion coefficient of Argon (1/K)
ΔT	Temperature difference between the inlet & outlet of PVT collector (-)
ε_g	Emissivity of the glass cover (-)
ε_{PV}	Emissivity of the PV module (-)
γ	Tilted azimuth (°)
δ	Thickness (m)
ϕ	Latitude (°)
η	Efficiency (%)
μ_w	Dynamic viscosity of water (kg/m s)
υ_{arg}	Kinematic viscosity of Argon (m³/s)
ρ_d	Diffuse reflectance of the cover plate (-)
ρ	Density (kg/m³)
σ_M	Von Mises stress (MPa)
σ	Stefan-Boltzmann constant (= $5.67 \cdot 10^{-8}$ W/m² K⁴)
θ_e	Incidence angle of the solar radiation (°)
τ_g	Transmittance of the glass cover (-)
τ_{PV}	Transmittance of the PV module (-)
$(\tau\alpha)_{PV}$	Transmittance-absorptance product for the PV module (-)

Subscripts

a	Ambient
abs	Absorber
arg	Argon (ideal gas)
b	Beam solar radiation
back	Back of the PVT collector
bond	Bonding
ca	From cover to absorber
cd	Conduction
cv	Convection
d	Diffuse solar radiation
e	Electrical
fi	Between pipe and fluid
fm	Mean fluid
g1	Outer glass cover
g1i	Inner glass cover
g2	PV glass cover
gro	Ground solar radiation
ins	Insulation layer
in	Mains water entering the water storage tank
longλ	Long wavelengths (2.5-40 μm)
o	Optical
out	PVT collector outlet
PV	PV cells
r	Reduced
ref	Reference PV cell values at an ambient temperature of T_a = 25 °C and a solar irradiance of G = 1 000 W/m² (K)
rd	Radiation
sky	Sky
shortλ	Short wavelengths (0.4-2.5 μm)
t	Total solar radiation
th	Thermal
top	Top of the PVT collector
u	Useful heat from the absorber to the water
w	Water
wind	Wind

1. Introduction

The integration of renewable technologies in buildings can lead to a significant decarbonisation of the energy system, lowering the current reliance on fossil fuels and the associated emissions from their combustion. Solar energy has the potential to play a leading role in such an energy solution. It addresses the energy problem simultaneously from human health, environmental, economic and security perspectives, and is quickly approaching grid parity in high-irradiation regions. Moreover, solar energy is capable of satisfying both the electrical and thermal needs of buildings and end-users, by means of Photovoltaic (PV) and Solar Thermal (ST) technologies respectively or, more recently, hybrid Photovoltaic-Thermal (PVT) systems that synergistically combine the characteristics and advantages of PV and ST systems.

It has been noted that the one the most desirable aspects of PVT technology arises from its more efficient and attractive use of roof space compared to stand-alone PV and ST collectors [1–3]. Where there are space constraints, PVT systems that can generate both electricity and a useful thermal output simultaneously from the same area and with a higher overall efficiency compared to separate stand-alone systems [4,5]. Thus these systems appear as highly suitable solutions for combined energy (heat and power) provision [6,7], especially where opportunities exist to implement solutions that must cater to diverse multi-vector energy demands. In particular, PVT-water (PVT-w) systems have been shown to be capable of higher electrical efficiencies compared to PV modules, by up to ~15%, while also generating Domestic Hot Water (DHW) and/or providing space heating. Consequently, PVT-w technology is considered to have an especially important potential in the residential sector [1,2,8–10], where a thermal-energy demand exists that accounts for 60-90% of the total energy demand in buildings in cold climates, and 30-40% in warmer climates [11], and where there is also electricity demand throughout the year [12]. Previous research undertaken by the authors concluded that PVT-w systems can cover up to about 50% of the total electricity demand, and 35-50% of the DHW demand of a typical household in London (UK) [6,12], while fully covering the electrical demand and ~70% of the DHW demand of a household in Larnaca (Cyprus) [13].

Commercial PVT collectors are marketed based on their high overall/total efficiencies (up to 70-80% claimed for some designs [1]), which establish this technology as an interesting option for integration in buildings. However, there are still very few PVT manufacturers and installers [14], and most products available on the market are not based on designs optimised specifically for PVT applications. Reviews of the state of innovation and R&D progress of PVT technology have highlighted the need to optimise the geometrical design of PVT collectors in order to enhance their performance [15], as well as to propose new thermal-absorber configurations [1,8]. At the same time, there is a strong drive for significant cost reductions to all ST technologies [16]. The International Energy Agency (IEA) has set a new task on PVT collectors (Task 60) under the Solar Heating and Cooling (SHC) programme which aims, among others, to improve the testing, modelling and adequate technical characterization of PVT collectors to boost the correct inclusion of PVT technology in simulation software, and to explore potential cost reductions in the balance of systems [17].

The main aim of the research reported in this paper is to propose improved PVT collectors with an optimal balance of energy efficiency, weight/strength, cost and ease of manufacture, specifically by considering new polymeric absorber-exchanger configurations with geometrical designs that significantly reduce weight and cost relative to conventional (copper sheet-to-tube) designs, while maximising heat transfer and thereby improving or at least maintaining the overall (thermal and electrical) efficiency of the collectors. One drawback of polymeric collectors arises from the exacerbated thermal expansion and lower mechanical strength of polymers, which makes structural and thermal expansion analyses of particular importance.

Hybrid PVT collectors operate over a range of temperatures throughout a day, also depending on the solar irradiance and ambient temperature, and therefore on the location, with temperature differences between day and night of more than 60 °C. This temperature variation leads to thermal expansion stresses, which should be evaluated to ensure that the deformations in the collector structure, and specifically in each PVT material layer, are within permissible limits thereby avoiding structural failure. Typically, the most critical layers in a hybrid PVT collector are the encapsulation material and the PV cells. Similarly to PV modules, the encapsulation material is a critical component as it provides structural support, electrical isolation,

physical protection, optical coupling and thermal conduction for the solar cell assembly [18,19]. The most common encapsulation material used in a wide variety of PV modules is elastomeric polymer. However, there is a significant difference between the thermal expansion coefficients of polymers and silicon cells, which leads to stresses throughout a diurnal cycle and can cause fractured cells, cracks and separation of the encapsulant, or broken interconnections [20]. Therefore, the encapsulant material should be able to accommodate the thermal expansion of the different materials without overstressing the PV cells and interconnections, and must be resistant to fracture. Furthermore, the material should also have a low cost and be easy to manufacture, a high optical transmission, low water absorption and permeability, a high resistance to UV degradation and thermal oxidation, good adhesion, chemical inertness and high dielectric constant. The most common encapsulant material used is Ethylene Vinyl Acetate (EVA) [20], however, this encapsulant loses its mechanical properties at 130-140 °C and as a consequence can delaminate [20–22].

Meanwhile, PV laminates used in PVT collectors have usually the same specifications as those used in commercial PV modules, which are certified to operate safely up to 85 °C according to the IEC 61215 standard [21,22], so in PVT applications the PV cells can suffer damage under rapid thermal expansion due to stress variations. In previous studies into the failure modes of PV modules [20], delamination at interfaces, water penetration, short circuits, cell interconnection failures and cracking of the solar cells from expansion/contraction stresses were identified, among others, as early failure modes.

Despite their importance, few studies in the literature to date are concerned with the effects of thermal stresses in PVT collectors, and those that address this topic focus mainly on overheating and stagnation phenomena [21,23–26], rather than on the assessment of structural deformations and their effects on the different layers of a PVT collector. Most studies that address fatigue characterisation or performance requirements and loads focus on ST systems [23,26], and those that consider the most critical layers (EVA encapsulant and PV cells) focus on PV modules [20]. Although the effects of high temperatures and thermal expansion are somewhat similar to ST and PV collectors, the conclusions of these studies should not be extrapolated to PVT collectors as the cooling effect of the liquid leads to different temperature gradients throughout the collector length in the various layers, and particularly the PV cells. Undertaking experimental studies to analyse thermal expansion and associated loads is expensive and complex, so a detailed theoretical model that incorporates the different materials and layers is important in identifying the critical components on which further, specific experimental considerations might be required.

A number of 3-D CFD analyses have been undertaken in this context, mostly on flat-plate ST collectors [27–31] or solar air heaters [32]. For example, a polymeric ST collector was modelled by CFD in Ref. [27] providing insight on the velocity field and pressure drop inside the collector channels. Nevertheless, very few papers have been found that analyse the performance of PVT collectors through 3-D CFD and FEM analyses. In particular, Refs. [33,34] consider copper sheet-and-tube (parallel tubes) PVT collectors, and the analysis focuses on the temperature and water flow distribution, so it would be of interest to extend these by addressing the thermal expansion and associated strains that PVT collectors suffer.

The mechanical properties of the absorber-exchanger component of a PVT collector are important for supporting the collector loads in the short term, such as due to wind, as well as in the long term, i.e., creep resistance, at high and low temperatures. In particular, toughness or ductility are important in determining the collectors ability withstand thermal expansion or mechanical torsion without brittle failure. Failure due to cycling loads and fatigue, can be caused by growth of crack tips or concentration of stresses in imperfections within the polymer [20], thus it is also necessary to identify high temperature (i.e., hot) spots and/or stress concentration areas, which might be especially vulnerable to continuous temperature gradients throughout the day and to high temperatures close to stagnation.

PV cells operating at a higher temperature or lower irradiance are known to generate a reduced electrical output, specifically, a lower voltage in the former case and a lower current in the latter [35]. Therefore, a detailed spatially-distributed PVT collector model is required to predict accurately the non-uniform temperature distribution over the solar cells and, ultimately, the performance of the whole collector. In previous work by Guarracino et al. (2016) [13], a 3-D PVT model demonstrated a temperature variation

amounting to ~10 °C over the surface of a sheet-and-tube PVT collector at normal operating conditions. This variation led to a 5% drop in the efficiency of cells at the identified hot regions compared to the cooler areas of the collector, and a corresponding loss in the collector's electrical performance. Thus, one objective here is to use the 3-D PVT model in order to identify any hot regions, and to use this knowledge to design a module that attains uniform cooling by eliminating these as far as possible.

In this work, a commercially available sheet-and-tube PVT collector (ECOMESH panel) is modelled in COMSOL and validated against experimental data provided by the manufacturer. Once a COMSOL model of this commercial PVT collector has been developed and validated, the model can then be used with confidence to evaluate the thermal performance of a range of alternative absorber-exchanger geometries in the same collector. The 3-D graphic capabilities of COMSOL facilitate the modelling of complex geometries that would not have been easy to model otherwise. Furthermore, COMSOL allows us to assess the thermal expansion of the absorber-exchanger due to temperature variations in the different material layers, which is of particular importance when polymeric materials are considered. Specifically, in the present paper we focus on the overall thermal performance of 28 alternative absorber-exchanger designs (including several flat-box and sheet-and-tube designs), followed by the detailed analysis of the temperature distribution over the promising PVT collector alternatives during operation. This insight into the associated thermal stresses and structural deformation experienced by these collectors is necessary for ensuring adequate performance throughout their predicted lifespans.

In what follows, the motivation for selecting the shortlist of PVT designs considered in this work is given in Section 2. The specifications of the modelled PVT collector, employed methodology, assumptions, initial conditions and other such considerations are given in Section 3. Section 4 contains the main results and an associated discussion including model validation, parametric analyses, performance curve assessment, structural characterisation and technoeconomic analysis. Finally, Section 5 summarises the main conclusions from this investigation. Further details of the numerical model can be found in Appendix A.

2. Hybrid PVT collector selection

As stated by other authors [15,35,36], the use of liquid-phase heat-transfer fluids with their higher heat capacities and heat transfer coefficients compared to air increases the heat transfer rate for PV cooling and allows a more efficient use of the captured thermal energy with reduced temperature fluctuations. Amongst the various potential liquid substances for PVT applications, water is by far the most commonly employed fluid [35,36]. Hence, it is no surprise that significant research has been dedicated in recent years to a number of PVT water (PVT-w) systems covering material selection, design and operation [1,2,15,37]. In these PVT collectors, copper is the most widespread solid material used for several reasons including, primarily, its high thermal conductivity, and the sheet-and-tube arrangement is the most common absorber-exchanger design found in literature and employed in commercially available PVT collectors [6,38–42]. Beyond the heat exchange configuration, several collector designs have been considered [1,7,40], including uncovered (unglazed), with one or two glass covers (glazed), with or without a gap between the cover(s) and PV cells, filled with air, other inert gases or even a vacuum (evacuated). Previous work [7,43] concluded that the use of inert gases is promising, as this significantly reduces the convective heat-loss from the top surface (in the case of Argon, 27.6% lower than the equivalent for air, which leads to an improvement in the overall heat-loss coefficient of around 4.8% for Argon). Consequently, it was decided here to use the commercial ECOMESH panel [44] as a benchmark reference case. This collector has nine copper parallel riser tubes and an innovative cover filled with inert gas, which improves significantly the collector's thermal performance while maintaining a high electrical output.

In an attempt to improve the bonding quality and heat transfer of PVT collectors, some alternative absorber-exchanger designs such as the flat-box structure made of extruded aluminium alloy have been proposed [38,45,46]. The present research considers an aluminium alloy flat-box structure as a first alternative to the reference case, with the aim of reducing the weight and cost of the absorber-exchanger, while improving (or at least maintaining) the thermal efficiency of the collector. In addition, this research proposes new absorber-exchanger flat-box designs made of polymer, as it is believed that

some polymeric materials have properties that make them an interesting option for PVT collectors [37,47], including their low density, good mechanical strength, lack of need for special surface treatments, corrosion resistance, ease of mass production manufacturing with the additional benefit of having fewer components to assemble, and lower production cost thanks to the low-cost material and reduced manufacturing time. Nevertheless, some properties of polymers, such as their lower thermal conductivity, large thermal expansion and limited service temperature, are disadvantageous for this type of application [37]. The ideal polymer should have high UV, water and glycol resistance/compatibility, good chemically stability, high thermal conductivity, good thermal range of utilisation (-10/+150 °C) and good mechanical strength [47–49]. With this in mind, two polymers are proposed: i) polycarbonate (PC), as suggested by previous authors [48–50], and ii) polyamide (PA), without and with additives to improve its thermal conductivity [51], which have not been previously considered to the best knowledge of the authors. A few polymeric flat-box designs have been previously considered; for instance, Huang et al. (2001) analysed channels of size 6×4 mm (W×H) [50], while Cristofari et al. (2009) studied larger channels of size 10×10 mm (W×H) based on the results of parametric analysis undertaken in previous work [48] in which it was concluded that the highest thermal energy gain is achieved by a collector with a channel height of 1 mm but that a fluid layer thickness of 10 mm can collect more than 90% of the maximum thermal energy gain of the smaller channels. Finally, a conventional aluminium sheet-and-tube PVT collector configuration is also studied here in order to benchmark the performance of the alternative absorber-exchangers proposed here, both in terms of material and design.

Thus, the main contributions of the present research include: i) the consideration of an innovative high-efficiency PVT collector featuring a cover filled with inert gas (ECOMESH panel), ii) the development and validation of a detailed 3-D FEM and CFD model of the PVT collector involving multi-physics processes (heat transfer, fluid dynamics and solid mechanics), iii) the assessment of a range of flat-box designs and materials (copper, aluminium, PC, PA with and without additives), all implemented within the same reference 3-D PVT collector model for benchmarking and comparison purposes, iv) beyond the technoeconomic assessments, thermal stress and structural deformation analyses of the proposed PVT collectors, which are crucial for ensuring long lifetimes and especially important in the case of polymeric collectors.

3. Methodology

Each absorber-exchanger design is defined by a series of geometrical parameters and material properties in COMSOL and energy balances are solved considering simultaneous radiation, convection and conduction between all collector layers. Firstly, the reference PVT collector design is modelled and the results are validated against experimentally-derived performance curves provided by the collector manufacturer (EndeF Engineering). The other designs are then modelled by using the same model with modifications implemented to describe each specific alternative absorber-exchanger geometry and construction material. From the fluid temperature rise and heat flux obtained from the simulations over a range of steady-state operating conditions, it is possible to evaluate the optical efficiency (η_o), and linear and quadratic heat-loss coefficients (a_1 and a_2). These are the characteristic parameters used to compare the thermal performance of PVT collectors according to the European standards for solar collector testing [52]. It is noted that in our simulations the PV electrical power output is also modelled in the PVT collectors and reported (see Figure 16), but the main focus of the present work is on the collectors' thermal performance so details on the electrical efficiency are only provided in the last analysis (see Section 4.5). Finally, a simple cost analysis is undertaken to assess the various configurations also from an economic perspective, for the case of Spain, which could be generalised to any country or region with similar natural gas and electricity prices.

3.1 PVT collector modelling

The PV cells and the thermal absorber are the two main components of a PVT collector. In Figure 1, the components of the collector are shown in detail: glazing, PV cells, EVA and Tedlar layers, absorber-exchanger (which corresponds to the thermal absorber and the riser water tubes/channels) and the insulation. In order

to evaluate the heat flux throughout the collector and obtaining the temperature distribution, the energy balance equation is applied to each of the collector layers [6,40,53]. In this way, the average temperatures of all the separate collector layers are estimated. The main heat transfer mechanisms are radiation (from the glass and the PV module to the sky, and the surface to surface radiation between Glass 1 and Glass 2), convection (from the outer surfaces to the ambient, within Glass 1 and Glass 2, and from the tubes/channels to the heat transfer fluid) and conduction (between all solid layers). See Appendix A for a full list of equations.

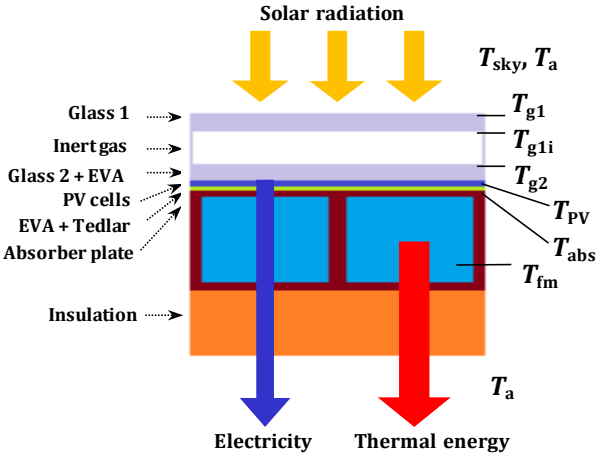

Figure 1. PVT collector cross-section for the flat-box design, showing the various collector layers (not to scale).

The PVT model is developed under the following assumptions:

- the absorption in the glass layers ('Glass 1' and 'Glass 2' in Figure 1) and in the frame are neglected [54];
- the ambient temperature is considered uniform around the collector [47,53] and heat losses from the sides of the PVT collector are negligible [53];
- solar irradiance and wind speed are uniform over the collector's surface area;
- the temperature dependence of the material properties of all solid components is neglected;
- the total water mass flow-rate is distributed uniformly amongst all collector riser tubes [47,55];
- free convection in the tubes is neglected;
- radiative thermal exchanges between the sides of the collector channels are neglected [41,47,56,57].

The model is run under steady-state conditions [40,58].

In the case of detailed 3-D CFD-FEM simulations where there are multiple radiating surfaces and heat transfer mechanisms, and where fluid-dynamic equations should be solved simultaneously, as in the case of a hybrid PVT collector, the significant amount of time and computational resources required for the simulations becomes a challenge. Moreover, the particular collector geometries considered here have high aspect ratios, with pipe lengths (L) being of the order of 1 m, while the thicknesses of the various transverse layers are of the order of 10^{-4} m, which complicate the meshing. For this reason, a swept mesh is used instead of a tetrahedral mesh as it fits better the geometries of interest and generates a structured mesh with higher element quality. To verify that the mesh selected does not lead to numerical inaccuracies, a convergence study over a range of mesh element sizes is also performed (see Section 4.1.2).

Furthermore, in order to reduce the computational cost without simplifying the physics (which would reduce the model accuracy) simplifications are made where possible, in particular by considering the inherent symmetry of the considered problems, i.e., designs, boundary conditions. In this work, it is assumed that the total cooling water flow-rate is divided equally amongst all collector channels, both in the case of the parallel fluid channels in the flat-box structure and in the sheet-and-tube (rise pipes) collector design [47,55], and therefore symmetry is applied to solve this problem with reduced computational cost. For example, in the case of the sheet-and-tube design under the assumptions of negligible side losses, uniform flow-rate and uniform inlet temperature into each tube, the heat transfer problem is solved for

only one-half of a riser tube and the temperature profile is considered to be symmetric. Therefore, symmetry boundary conditions have been applied along the centreline of the sheet-and-tube PVT collector, thus only half-pipe and half-fin collector sections have been implemented in the COMSOL models [59].

The geometry of the flat-box structure is simpler to model, given its rectangular nature. In this work, we consider a single whole channel for higher aspect-ratio designs (20×10 mm and 40×10 mm) and two whole channels for lower aspect-ratio designs (10×10 mm, 6×4 mm and 3×2 mm), as shown in Figure 2.

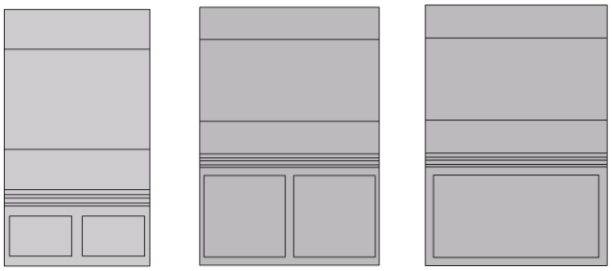

Figure 2. Cross section of: (left) two 6×4 mm channels, (middle) two 10×10 mm channels, and (right) one 20×10 mm channel for the flat-box structure configuration as modelled in COMSOL.

Since there is currently no standard method to assess the performance of PVT collectors [3], both the ASHRAE [60] and ISO [61] characterisation approaches for ST collectors are followed in order to report and to compare the thermal efficiencies of the different PVT collector and absorber-exchanger designs.

The ASHRAE method is based on the heat removal factor (F_R) and the overall heat-loss coefficient (U_L) of the collector [3], which can be obtained by calculating the thermal efficiency of the collector at different inlet temperatures at steady-state conditions [62,63],

$$\eta_{th} = \frac{q_u}{I_t} = F_R(\tau\alpha)_{PV} - F_R U_L \frac{T_{in} - T_a}{I_t}, \quad (1)$$

where η_{th} is the thermal efficiency of the PVT collector, q_u is the useful thermal energy extracted (W/m^2), I_t is the total solar irradiance per meter square (W/m^2), $(\tau\alpha)_{PV}$ is the combined transmittance-absorptance coefficient, T_{in} is the inlet water temperature and T_a is the ambient temperature.

In the ISO method, the collector is also tested under steady-state conditions but in this case the difference between the mean fluid temperatures (T_{fm}) and ambient temperatures (T_a) is considered [3,7,43],

$$\eta_{th} = \frac{q_u}{I_t} = \eta_o - a_1 T_r - a_2 I_t {T_r}^2, \quad (2)$$

$$T_r = \frac{T_{fm} - T_a}{I_t}, \quad (3)$$

where η_o is the optical efficiency, a_1 is the heat-loss coefficient which accounts for the linear heat-loss variation, a_2 is the temperature dependence of the heat-loss coefficient which accounts for the quadratic heat loss variation, T_{fm} is the mean fluid temperature and T_r is the reduced temperature.

The PV electrical efficiency varies linearly with the cell operating temperature as [6,64],

$$\eta_{PV} = \eta_{ref}[1 - \beta_0(T_{PV} - T_{ref})], \quad (4)$$

where η_{ref} is the reference module efficiency at a PV cell temperature, T_{ref}, of 25 °C and at a solar irradiance of 1,000 W/m^2 (value given by the manufacturer), and β_0 is the temperature coefficient for the PV module, also given in the technical specifications of the ECOMESH panel being considered.

A parametric analysis with the aim of selecting the most promising design(s) for the two absorber-exchanger designs (sheet-and-tube, flat-box) is also undertaken. A range of pipe diameters and number of riser tubes for a fixed total collector width (B) are investigated for the sheet-and-tube design, considering both copper and aluminium as material, and a range of polymeric materials, copper and aluminium as well as different channel dimensions are considered for the flat-box configuration.

3.2 PVT collector parameters

In this work, the commercial ECOMESH panel [44] is selected as the reference PVT collector. Similarly to Figure 1, this collector comprises (from top to bottom): i) a transparent glass cover and insulating gas layer [43], ii) a multi-crystalline silicon PV module, iii) an EVA encapsulating film, iv) an absorber-exchanger which transfers heat to the heat transfer fluid, and v) an insulation layer. The absorber-exchanger consists of a sheet-and-tube heat exchanger in which the heat transfer fluid (water) flows through nine parallel copper pipes. The external diameter of the pipes is 8 mm and the heat transfer coefficient is 400 W/(m·K) [7]. The PVT collector has a nominal (peak) electrical power of 240 W_p, total aperture area of 1.55 m^2, nominal PV module efficiency of 14.7%, and a PV temperature coefficient of -0.45 %/K. The recommended collector flow-rate range is 10-50 L/h, with 30 L/h taken as the nominal value [44]. In the present work, all PVT collector parameters relating to its different layers are kept constant (dimensions, cover layers, PV cells, etc.), only varying the parameters associated with the absorber-exchanger, for comparison purposes.

As a first alternative to the reference case, considering the results of the parametric analysis in Section 4.2, six different copper sheet-and-tube designs are studied, with three different riser-tube diameters (6, 8 and 10 mm) and three different number of riser tubes (9, 12 and 18 tubes). Additionally, to study the influence of the material on the performance of the PVT collector, four of the previous sheet-and-tube designs are modelled using aluminium alloy as the solid material.

A number of different flat-box structure designs are considered as potential alternatives to the sheet-and-tube designs. In particular, 3 channel dimensions are studied, i.e.: 20×10 mm (W×H) as suggested by several authors [38,65,66], 10×10 mm and 3×2 mm, all constructed from aluminium alloy. In addition, two polymer types are considered for the absorber-exchanger: PC and PA. Some variations of the latter with different loadings of hexagonal boron nitride (hBN) particles (additive) are also studied [51]. The physical and mechanical properties of the different proposed materials are summarised in Table 1.

Table 1. Physical and mechanical properties of the different materials considered.

Properties	**Density, ρ (kg/m^3)**	**Thermal conductivity, k (W/(m·K))**	**Specific heat capacity, c_p (J/(kg·K))**	**Young's modulus (GPa)**	**Poisson's ratio (-)**	**Thermal expansion coefficient, ×10^{-6} (1/K)**	**Yield stress (MPa)**	**Ultimate tensile stress (MPa)**
Tempered Glass[1]	2,210	1.40	730	70	0.22	9	750-2,130	180
EVA[2]	960	0.35	2,090	0.018	0.32	350	-	26
Tedlar[3]	1,250	0.36	1,200	2.34	0.40	75	38	55-110
PV module (silicon)[4]	2,329	130	700	170	0.28	2.6	3,200-3,460	160-180
Copper[5]	8,700	400	385	110	0.35	17	230	287
Aluminium alloy[4]	2,702	237	903	75	0.33	22	265	300
PC[6]	1,180	0.78	1,200	2.35	0.38	68	59-70	55-75
PA30-33[7]	1,390	3.60	1,700†	2.9	0.36	51	50-95	90-165
PA	1,140	0.26	1,700†	N/A	N/A	N/A	N/A	N/A
PA90-15[7]	1,170	1.20	1,700†	N/A	N/A	N/A	N/A	N/A

[1] *(MakeItFrom.com);* [2] *Ref.* [68]*;* [3] *(GoodFellow);* [4] *Ref.* [70]*;* [5] *Ref.* [71]*;* [6] *(GoodFellow);* [7] *Ref.* [51].

† *The same heat capacity is considered for all PAs as the addition of hBN does not significantly influence this physical property and its effect on the absorber-exchanger performance (within this order of magnitude) is negligible.*

Table 2 summarises all the different design materials and dimensions considered in the present research, which were selected from the literature and from our own results detailed in Section 2.

Table 2. Summary of the absorber-exchanger designs studied. Here, D refers to external diameter and n to the number of riser pipes.

Sheet-and-tube		**Flat-box structure**			
Copper	**Aluminium**	**Copper**	**Aluminium**	**Polymer**	
D* = 8 mm, *n* = 9	*D* = 8 mm, *n* = 9	3×2 mm	3×2 mm	PC	PA90-15
D = 6 mm, *n* = 9	*D* = 10 mm, *n* = 9	10×10 mm	10×10 mm	- 3×2 mm	- 10×10 mm
D = 10 mm, *n* = 9	*D* = 8 mm, *n* = 12		20×10 mm	- 6×4 mm	PA30-33
D = 8 mm, *n* = 12	*D* = 10 mm, *n* = 12			- 10×10 mm	- 3×2 mm
D = 10 mm, *n* = 12				PA	- 6×4 mm
D = 8 mm, *n* = 18				- 10×10 mm	- 10×10 mm
				- 20×10 mm	- 20×10 mm
				- 40×10 mm	- 40×10 mm

* *Reference case is highlighted in bold.*

The same initial conditions are applied to all considered PVT collector designs at steady state, i.e.: a total incident solar irradiance (I_t) of 1000 W/m^2, ambient temperature (T_a) of 25 °C, mains water temperature (T_{in}) of 20 °C, and PVT collector tilt angle (β) of 35°. It should be noted that two collector flow-rates are considered: a nominal flow-rate specified by the PVT manufacturer of the reference PVT collector, 30 L/h (8.3×10^{-3} kg/s), which is used for all sheet-and-tube configurations, and the optimal flow-rate for the 10×10 mm flat-box configuration according to Refs. [47,48], 19.2 L/h (5.3×10^{-3} kg/s), which is used for all flat-box configurations. Furthermore, the latter optimal flow-rate is also considered in the reference PVT collector to compare it with the flat-box alternatives under the same operating conditions.

3.3 Structural analysis

To complement the aforementioned analysis, 3-D FEM and CFD modelling is used and solid mechanics is added to undertake a structural analysis of the most promising absorber-exchanger designs. As discussed previously, the significant amount of both time and computational resources required for detailed 3-D FEM-CFD simulations makes it necessary to apply some simplifications to simplify the problem (even though this slightly reduces the accuracy of the 3-D model, as discussed below). As stated previously, it is assumed that the water mass flow-rate is divided equally among all tubes of the collector [47,55], such that symmetry can be used to simplify this problem. Thus, only two channels are modelled (in the flat-box configurations), reducing significantly the computational time and resources. To verify that the number of modelled channels do not influence the results, simulations were run with 2, 5, 10, 15 and 20 channels, obtaining the same results (within numerical error), when the same boundary conditions were applied.

For the structural analysis, additional boundary conditions and constraints are required to specify how the PVT collector is held within its frame and overall structure. It is assumed that the PVT collector is completely fixed with the frame at the collector water inlet, while at the collector water outlet the frame has some tolerance, allowing expansion in the flow direction (*y*-direction) and along the collector width (*x*-direction) but not allowing displacement in the *z*-direction (collector height) (see Figure 3).

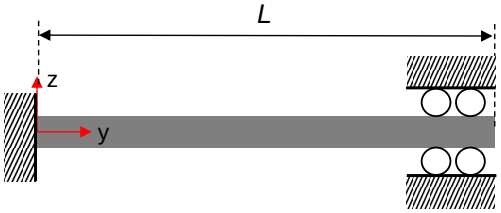

Figure 3. Sketch of the PVT collector (length L) inlet (fixed) and outlet (prescribed displacement) supports.

Due to the possible reduced accuracy expected from the introduction of the above modelling simplification (i.e. modelling two channels), a full 3-D analysis was also undertaken in order to understand the limits of the simplified model. The 3-D analysis demonstrated that, when considering the full 3-D problem, the maximum stresses suffered by the PVT collector are lower than those obtained above, which can be used as conservative limits. To this end, the cover glass was selected for closer inspection, since this is the layer with smaller temperature gradient and therefore smaller thermal expansion, which, as it will be shown later, leads to a reduction in stresses and therefore material issues. It is also the layer that experiences the highest stresses due to its weight, and thus the one most affected by the boundary conditions set on the lateral sides as shown below. Thus, the whole cover glass (0.948×1.58 m) was modelled: i) with the lateral sides supported (i.e., set with a prescribed displacement) in order to model the case when this is held by the PVT frame (Figure 4 top), and ii) with the lateral sides unsupported (i.e., let free, displacement is allowed), as it is considered when modelling two channels (Figure 4 bottom).

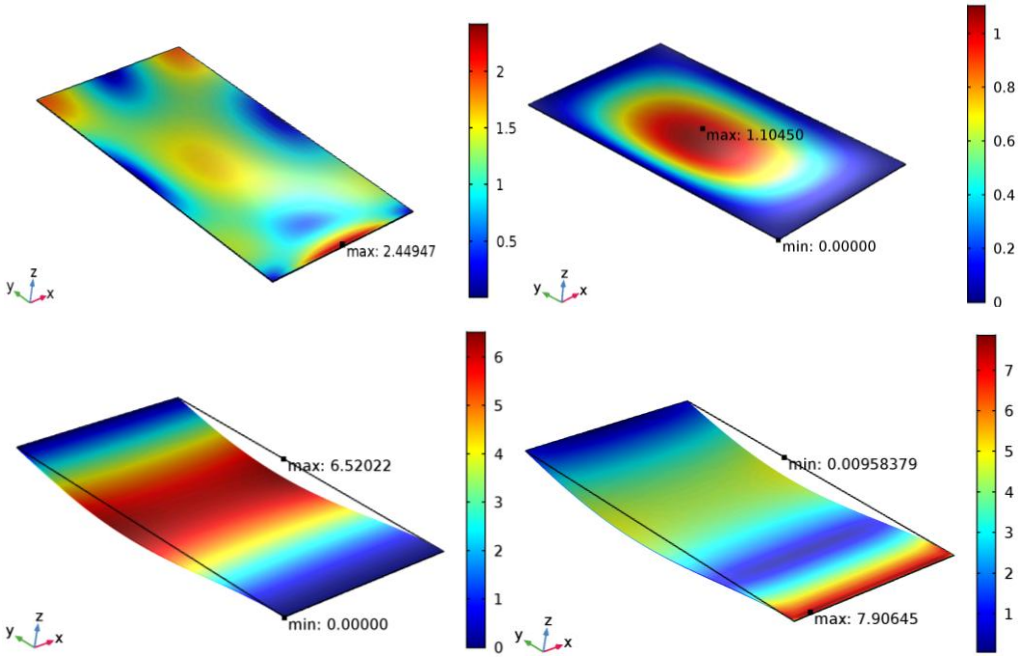

Figure 4. Whole cover glass (0.948×1.58 m) with the lateral sides: (Top figures) set with prescribed displacement (z displacement is not allowed but x and y displacement is allowed, COMSOL constraint: prescribed displacement); (bottom figures) let free, (displacement is allowed, COMSOL constraint: free). Figures on the left show von Mises stress (MPa), and on the right total displacement (mm).

The von Mises stress criterion (also called the equivalent or effective stress) [73–75] is used to evaluate whether the various PVT layers will yield when subjected to the strains associated with thermal expansion in normal operating conditions. The von Mises stress criterion can be formulated as indicated in Eq. (5), and it can be defined as the driving force for damage in many ductile engineering materials:

$$\sigma_{\mathrm{M}} = \sqrt{\frac{1}{2}\cdot\left[\left(\sigma_x-\sigma_y\right)^2+\left(\sigma_x-\sigma_z\right)^2+\left(\sigma_y-\sigma_z\right)^2+6\cdot\left(\tau_{xy}+\tau_{yz}+\tau_{xz}\right)\right]}. \quad (5)$$

The von Mises stress is routinely computed by COMSOL, and it is compared to the material's yield stress (or to the Ultimate Tensile Stress, UTS, when it is lower than the former, see Table 1), to determine whether each layer would yield or fracture. The maximum displacement due to deformation that the PVT collector suffers is also analysed; in this case this is defined as the percentage of the maximum displacement suffered by the collector over the total collector length.

The results for the cover glass analysis show that the effective stress suffered (von Mises stress) in the former case (i), more realistic, are significantly lower than in the second one (ii), being the maximum stress allocated on the same zone (see Figure 4 left), that is, the PVT collector water inlet, where the layers are fixed with the frame (left side of the Figure 3). Similarly, the largest displacement occurs in the *z*-direction due to the glass weight, being significantly higher, as expected, when the lateral sides are set free (see Figure 4 right). Therefore, the study undertaken in the present research is conservative in a way that it is expected that if the stresses obtained in the simulations are below the material limits, one could claim that the whole PVT collector will suffer less stresses than the ones shown in this work, so the designs proposed will perform correctly under the limits.

Consequently, and based on the results that showed that the dominant thermal expansion and associated stresses are expected in the *y*-/flow-direction due to the temperature gradient and in the *z*-direction due to gravity, the structural analysis of the PVT collector is simplified into a 2-D problem in the *y*-*z* plane.

3.4 Economic analysis

In order to undertake a simple cost analysis, the investment cost of each PVT collector design is estimated, and the financial benefits (savings) from the electricity and heat generation are converted to the same unit (€/h per PVT collector) and summed. To this end, the electricity and natural gas prices should be considered, whose corresponding values (€/kWh), in Spain, at the time of the research, are shown in Table 3, along with the prices of the materials and production costs of the proposed absorber-exchanger designs. The selected natural gas and electricity prices are within the range of EU utility prices [76] and thus the results can be generalised to any country or region with similar values.

Table 3. Cost factors used for the economic analysis for the case of Spain.

Cost analysis	**Value**	
Natural gas price	0.05[+]	€/kWh
Electricity price	0.14[+]	€/kWh
Polymer cost	2.3-3.0*	€/kg
Additive (hBN) cost	150[†]	€/kg
Aluminium 20×10 mm flat-box cost	2.33	€/m
Ratio copper/aluminium cost	1.27	-
Extrusion production cost	2	€/m

**Price varies slightly between this range for PA, PA30, PA90 and PC; [+] Refs.* [77,78]*; [†] Personal communications* [79,80]

The economic analysis presented here aims to estimate the payback time (*PBT*) of the collectors based on their investment costs (C_0) and cost savings (in €/h per PVT collector) as detailed in Eq. (6). Only capital costs are considered, without including transport or installation costs. For the *PBT* estimation, the same weather and operating conditions (as detailed in Section 3.2) are considered in all cases, thus leading to a simple figure that can be used for the intended comparison. The investment cost of the polymeric absorber-exchanger design is estimated from the cost of the raw material and the cost of adding the additive (hBN), where this is applicable, and also includes an estimation of the extrusion production cost. For the aluminium designs, the price of off-the-shelf square-channel tubes is considered [81], which is then extrapolated to the copper square channels considering the price ratio of both materials (Table 3).

$$PBT(\text{days}) = \frac{C_0(€)}{cost\ savings\ (€/\text{h}) \cdot 24\ (\text{h/day})}. \quad (6)$$

4. Results and Discussion

The 3-D COMSOL model of the reference PVT collector is first validated against experimental data provided by the manufacturer in Section 4.1.1. It is emphasised, as noted earlier, that the PV electrical power output

is also modelled and reported (see Figure 16), but our main focus is on the collectors' thermal performance so details on the electrical efficiency are only provided in the final analysis (see Section 4.5). The thermal efficiency, η_{th}, is plotted against the reduced temperature T_r, to obtain the coefficients η_o, a_1 and a_2 in Eq. (2) via data fitting. Mesh validation is then performed in order to find the optimal mesh for the CFD problem, aiming to reduce the computational time and resources as much as possible without losing accuracy in the results. Section 4.2 summarises the results of the parametric analysis undertaken for different pipe diameters in the sheet-and-tube design, which leads to the selection and more detailed study of a few potential designs that promise improved performance relative to the reference case. Efficiency curves obtained for selected absorber-exchanger designs are analysed in Section 4.3, followed by a structural analysis of a number of representative collectors in Section 4.4. Finally, results from a technoeconomic comparison of all proposed collector designs are discussed in Section 4.5.

4.1 Model validation

4.1.1 Performance curves from the 3-D model

The 3-D model developed in COMSOL is validated here against the manufacturer's experimentally-derived collector performance curve. To this end, the heat transfer problem was solved for the same ambient conditions (irradiance, wind speed, ambient temperature) and operating conditions (flow-rate, inlet fluid temperature) as specified in the manufacturer test report. The experimental data were obtained by testing the collector in steady-state conditions according to the international standards for solar collector testing EN 12975-2, as described in Ref. [52]. The collector's thermal efficiency (η_{th}) is plotted in Figure 5 against the reduced temperature (T_r). The 3-D model fits the experimental results with an average absolute deviation (AAD) error of 12%, over an inlet water temperature range of 0-80 °C. For inlet water temperatures below 60 °C, the AAD error is less than 15% (error bars in Figure 5), while the largest deviations appear at higher operation temperatures. This performance overestimation can be attributed to an underestimation of heat losses in the model, since the model assumes a perfect thermal contact between the PV cells and the rear copper sheet, and between the absorber and the pipe to which it is bonded. It is worth mentioning that Guarracino et al. (2016) [82] already reported that a poor contact between the PV module and the thermal absorber, leading to an insulating air gap between the layers, can reduce the thermal performance of the collector by up to 30%. Furthermore, heat conduction from the copper absorber to the tubes is modelled as a uniform bond made of copper with fixed dimensions along the entire length of the pipe, whereas in a real collector, and depending on the bonding method (welding, ultrasonic, etc.), this bond will vary. The material and dimensions of the bond strongly affect the heat conduction between the relevant layers and, therefore, the overall collector efficiency [83], as these two factors influence the heat removal factor (F_R) and overall heat-loss coefficient (U_L), and thus the PVT collector performance curve.

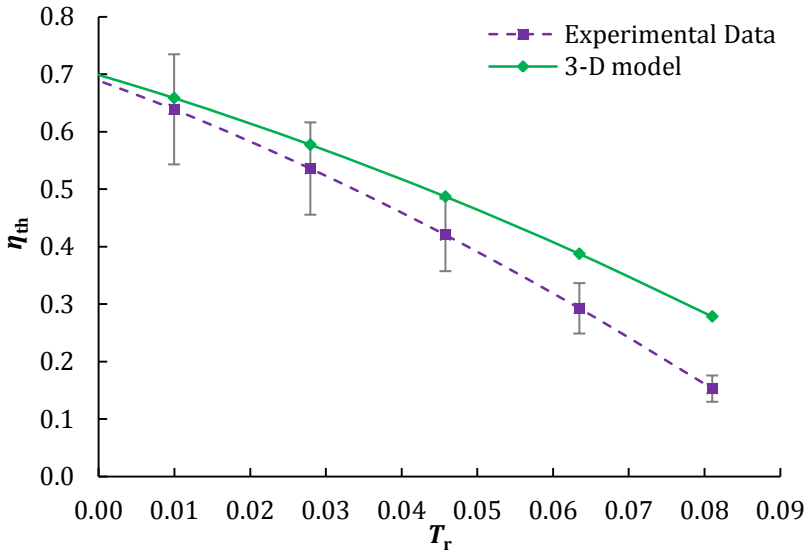

Figure 5. Performance curves of the reference PVT collector for the 3-D model and for the commercial ECOMESH panel (specifications sheet) [44]. *Results reproduced from previous work* [59] *and generated based on the conditions stated in Section 3.2.*

In addition, lateral and edge losses have not been considered here. Finally, it should be noted that the experimental performance curve is obtained from a scatter of experimental points, which might also result in some deviations of the reported curve from the range of actual experimental performance results.

4.1.2 Mesh independence

In order to optimise the computational effort and time required for the flat-box structure simulations, a mapped mesh for the cross section of the PVT channels (*x-z* plane) was selected, which takes advantage of the rectangular shape of the mesh elements. In a first approach, a simple uniform mesh was applied (*"NBL = 0"* in Figure 6). The mesh was then refined in the fluid domain inside the channel by adding points and also grid non-uniformity to capture the velocity gradients and the associated convective heat transfer from the surface of the solid into the fluid. As shown in Figure 6 (left), as the "Number of Boundary Layers" (NBL) in COMSOL was increased, more elements were added in the fluid domain, with smaller elements close to the surface and larger ones in the channel centre. The heat flux (W/m^2) into the liquid from the top of the channel (red line) for each of the studied meshes is shown in Figure 6 (right). The results show a deviation of less than 0.3% in all cases, with convergence from *NBL* > 8. The *NBL* = 0 mesh results were the same as those for *NBL* = 4, with a deviation of less than 0.1% relative to *NBL* > 8. Based on these results, and the significantly reduced computational resources required, it was decided to use the simplest mesh (*NBL* = 0) for this work (around 5 times faster than *NBL* = 8, with less than 1/3 of the RAM requirements).

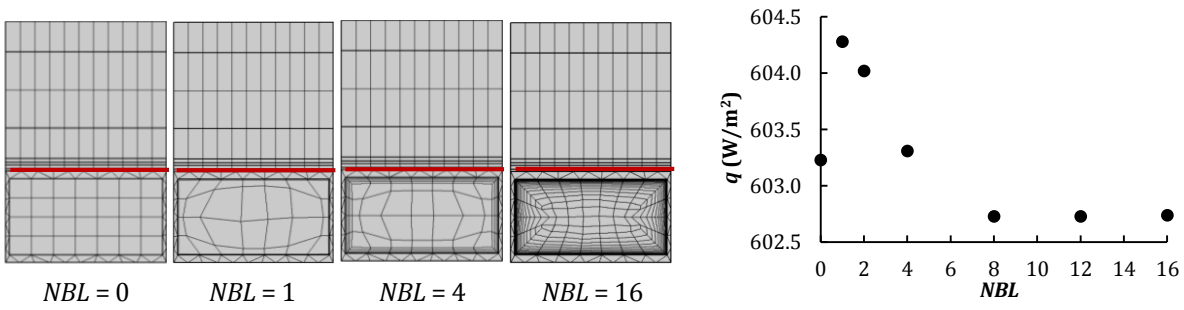

Figure 6. Mesh convergence for the 3-D flat-box structure model: (left) NBL = Number of Boundary Layers, and (right) corresponding q = heat flux (W/m^2) through the top of the channel (horizontal red line on left).

4.2 Parametric analysis

As an alternative to the reference collector, various sheet-and-tube designs were studied in an attempt to improve the efficiency of the PVT collector. To this end, a series of parametric analyses were performed for 5 different pipe diameters (D = 6, 8, 10, 12 and 15 mm), varying the number of riser tubes (n) from 2 to 100 pipes for a fixed total collector width (B = 945 mm), equal to that of the reference collector, hence varying the fin width (W) accordingly. The resulting W/D ratio varied from 0.80 to 80.

Figure 7 (left) shows that the pipe diameter D does not influence the thermal efficiency of the PVT collector, whereas an increase in the number of riser tubes n significantly increases both the thermal and electrical efficiencies up to about n = 20-30, beyond which the efficiency asymptotes, while the weight and cost of the PVT collector continues to increase, as is demonstrated in Section 4.5. This improvement is attributed to the cooling of the absorber and PV plates, allowing more heat to be extracted, which increases the thermal efficiency, while also reducing the maximum PV cell temperature reached between two adjacent pipes, therefore increasing the electrical efficiency. However, from around 20 riser pipes onwards the thermal and electrical efficiencies barely increase (see Figure 7 (right)), so it can be concluded that the slight improvement achieved at even larger n does not outweigh the associated increase in weight and cost. This result confirms the finding in Refs. [50,84,85], where a higher convective heat transfer between the coolant and the channels was achieved with reduced diameters and increased number of channels per unit width, leading to a consequent improvement in thermal efficiency, and also explains why the typical pipe width to pipe diameter ratios found in most sheet-and-tube collectors lies in the range 6-10 [50].

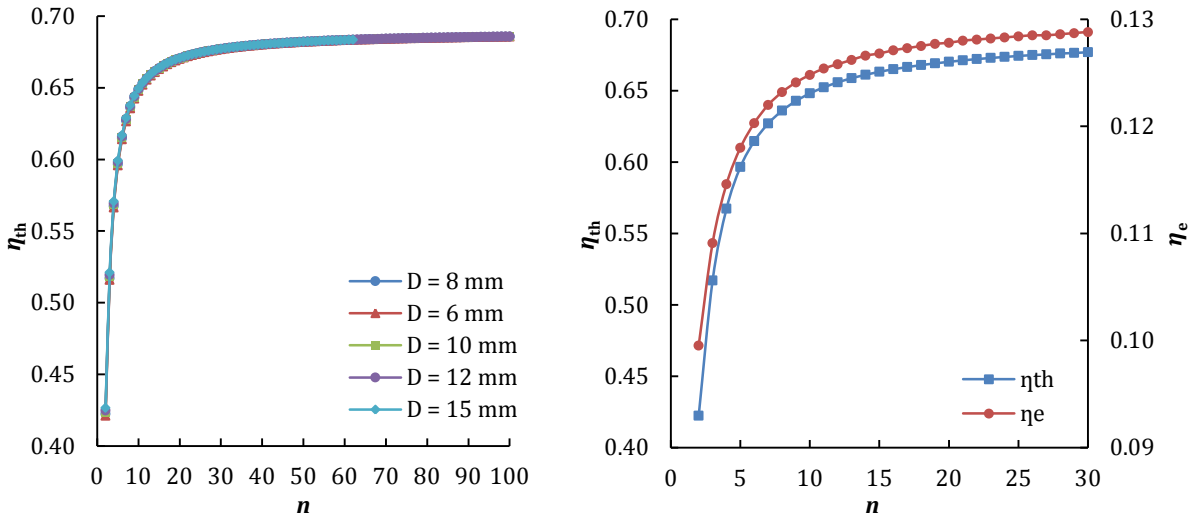

Figure 7. Effect of the number of riser tubes n on: (left) thermal efficiency η_{th} for different riser tube diameters D, and (right) thermal η_{th} and electrical efficiencies η_e for D = 8 mm. Results generated based on the conditions stated in Section 3.2.

Bearing in mind these results, performance curves for the following selected PVT collector designs were obtained by the detailed 3-D model in order to examine and compare their relative performance:

- For n = 9: D = 6, 8 and 10 mm – to study the influence of the pipe diameter;
- For D = 8 mm: n = 9, 12 and 18 – to study the influence of the number of pipes;
- For D = 10 mm: n = 12 – to confirm that the previous results also apply to a larger pipe diameter.

4.3 Performance curve analysis

Both the ASHRAE and ISO methods detailed in Section 3.1 were considered when comparing the thermal performance of the selected designs. As shown in Figure 8, similar results are obtained with both methods, so it was decided to use the ISO method (Figure 8 (left)) to compare the different designs, also because the ISO curves are less dependent on the collector flow-rate due to the fact that this method employs the

reduced temperature (T_r) that varies according to the flow-rate, as opposed to ASHRAE that only considers the inlet water (T_{in}) and ambient (T_a) temperatures such that different thermal efficiency curves are obtained for different flow-rates. The ASHRAE method is still used in this research to determine the heat removal factor (F_R) and the overall heat-loss coefficient (U_L) of the studied designs (see Figure 16).

Sheet-and-tube configuration. The thermal efficiency curves as a function of the tube diameter (D) for a number of tubes (n) varying between 9 and 18 are reported in Figure 8. The pipe diameter does not notably influence the thermal efficiency but doubling the number of riser tubes leads to an absolute increase in the thermal efficiency of 1.5%, or a relative increase of 2.3% (η_{th} = 67.4% for n = 18 *vs.* η_{th} = 65.9% for n = 9 for the same conditions, as given in Section 3.2). Similar results are obtained for aluminium, as shown in Figure 9. It is possible to observe that for the same design (same D and n), the copper sheet-and-tube performs better than the aluminium one, as expected, due to the higher thermal conductivity of the former. However, the reduction in price and weight of the latter may outweigh the very slight decrease in thermal performance of 1.2% (relative) (η_{th} = 65.9% *vs.* η_{th} = 65.1% respectively for n = 9 and D = 8 mm with conditions as in Section 3.2) as will be shown in Section 4.5.

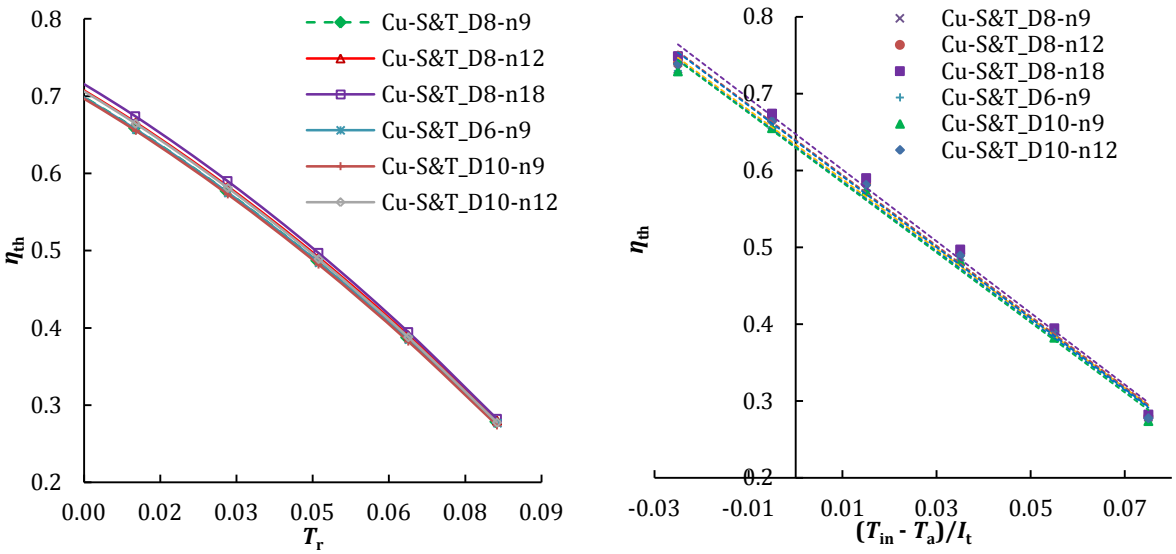

Figure 8. Performance curves of the different copper sheet-and-tube designs studied, considering (left) ISO (Eq. (2)) and (right) ASHRAE (Eq. (1)) methods. In the legend, for example, Cu-S&T_D8-n9, refers to 9 copper pipes with an external diameter of 8 mm. Results generated based on the conditions stated in Section 3.2.

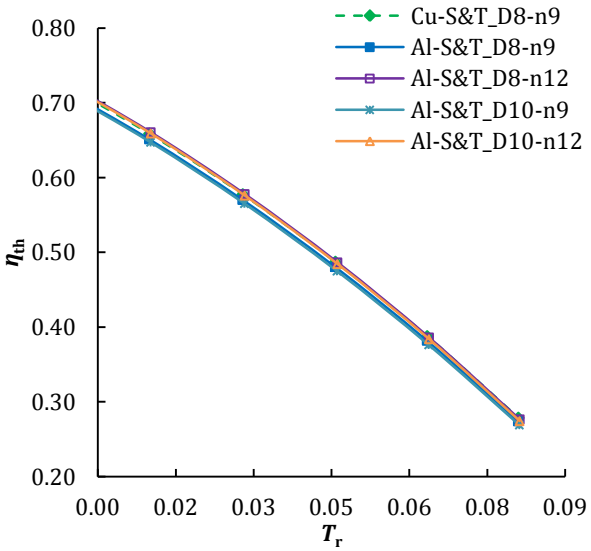

Figure 9. Performance curves of the different aluminium sheet-and-tube designs studied. In the legend, Al-S&T_D8-n9, refers to 9 aluminium pipes with an external diameter of 8 mm. Results generated based on the conditions stated in Section 3.2.

Flat-box configuration. Various channel dimensions and materials are investigated in conjunction with this collector configuration. A full list of flat-box PVT designs studied in this work is given in Table 3. Irrespective of the material and channel size, all the flat-box designs slightly outperform the reference copper-sheet-and tube design (Figure 10), since the heat transfer area between the absorber plate and the fluid is significantly larger than in the sheet-and-tube design, which outweighs the impact of the lower thermal conductivity of all the polymers considered here. As a consequence, the temperature on the top of the flat-box design is uniform and lower on average compared to the equivalent temperature observed in the sheet-and-tube design, leading to lower thermal losses (top thermal losses for the sheet-and-tube q_{top} = 144 W/m², while for the copper 10×10 flat-box, q_{top} = 109 W/m²). This result is in agreement with the results found by previous studies that used polymeric flat-box absorber-exchanger [47,56].

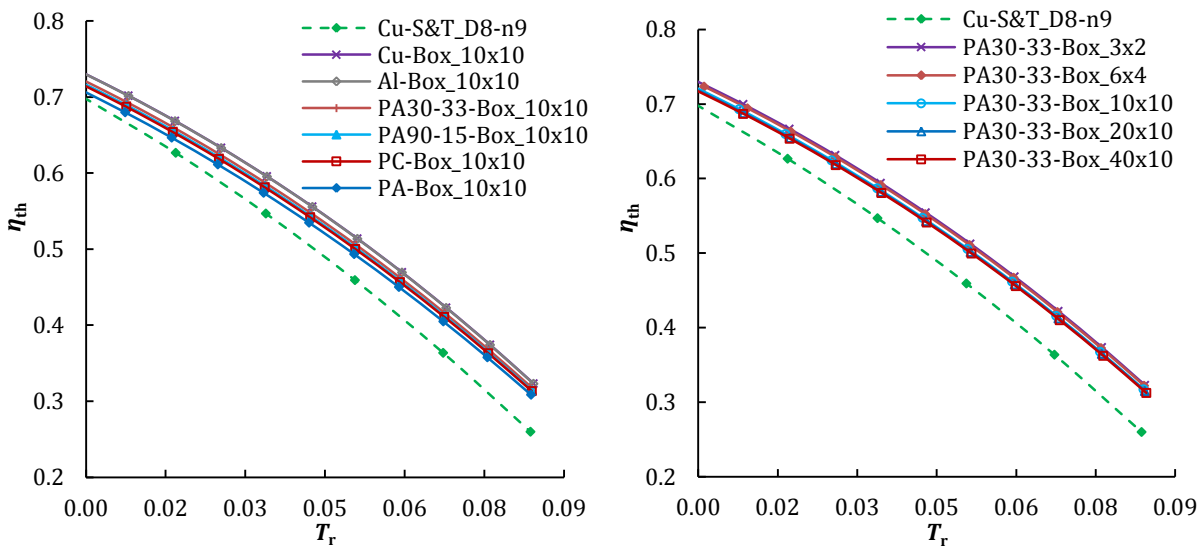

Figure 10. Performance curves of the different PVT designs studied for (left) same dimensions with different materials and (right) same material with different channel dimensions. Results reproduced from previous work [59] *and generated based on the conditions stated in Section 3.2.*

The effect of the flat-box solid construction material on the thermal efficiency of this configuration is assessed for PVT collectors with the same channel dimensions (10×10 mm) in Figure 10 left. It is observed that the optical efficiency (η_o) is higher by up to 4.3% and that the heat loss-coefficient (a_1) is lower by up to 15.5% compared to the sheet-and-tube collector, with the best performance achieved by the 10×10 mm channel designs. The difference in the performance curves between the best (made of copper) and worst (made of PA) flat-box design is less than 5% for the same channel dimensions. It should be highlighted the small thickness of the absorber plate (1 mm), leading to a small solid thermal resistance. Thus, the thermal performance of the PVT collector is less sensitive to the choice of material in this type of collector design.

As can be seen from the results in Figure 10 (right), for the same material, the channel dimensions also do not have a significant influence on the PVT collector thermal efficiency. The results show that the optical efficiency (η_o) can be increased by 4.6%, and the heat-loss coefficient (a_1) reduced by 15.5% relative to the reference case, when employing smaller channels. This is attributed to the higher water velocity through smaller channels given the smaller hydraulic diameters, since the total collector flow-rate is maintained constant in all the cases, which leads to higher convective heat transfer coefficients (h = 1 110 W/m² K for the best case (3×2 mm) *vs.* h = 170 W/m² K for the worst case (40×10 mm)). As a consequence, the temperature difference between the absorber plate (T_{abs}) and the fluid mean temperature (T_{fm}) is significantly smaller for the smaller channel designs.

From the results obtained relating to the flat-box configuration, the most promising PVT designs appear to have channel dimensions of 10×10 mm or lower. By analysing their efficiency for a range polymeric materials, it can be concluded that the small increase in thermal performance of the PVT collector might not outweigh the higher complexity and costs of loading the polymer with additives. Furthermore, the improvement achieved with the copper flat-box design relative to off-the-shelf polymers (e.g., PC or PA) for the same channel dimensions is small. When bringing into consideration the weight of the PVT collectors achieved with the proposed flat-box designs, Figure 11 shows that all the polymeric flat-box designs achieve a weight reduction of 7-12% compared to the reference case (Cu-S&T_D8-n9, red circle in Figure 11), whereas the aluminium flat-box collectors are 2-12% heavier (blue crosses) and the copper flat-box designs 48% (3×2 mm) and 59% (10×10 mm) heavier (light blue squares) than the reference collector, respectively. The absorber-exchanger accounts for 17.3% of the total PVT collector weight in the reference sheet-and-tube collector.

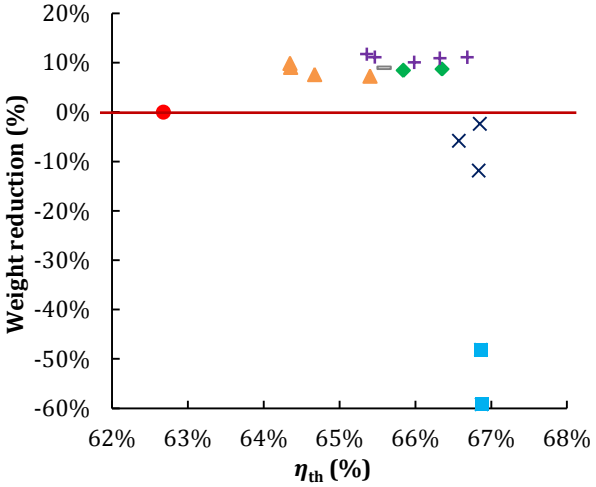

Figure 11. Percentage of weight reduction vs. thermal efficiency of the PVT collector for the different designs of flat-box design studied and the reference S&T collector. (Red circle = reference case, blue squares = copper flat-box, dark blue crosses = aluminium flat-box, green diamonds = PC flat-box, orange triangles = PA flat-box, grey line = PA90-15 flat-box, purple pluses = PA30-33 flat-box).

Bearing in mind these results, a structural characterisation as well as a technoeconomic analysis are required to bring into consideration other factors such as thermal expansion and stresses, PVT collector cost and payback time before more definitive conclusions are drawn.

4.4 Structural characterisation of the most promising and representative designs

This section summarises the structural analysis of the most promising and representative absorber-exchanger designs detailed in Table 4. The 3-D models were then run at steady-state with the initial conditions detailed in Section 3.2. Figure 12 shows the maximum von Mises stress values for the different layers of the PVT collector designs, providing an overview of which layers are suffering more strains. In addition, the stress distribution throughout different layer surfaces, which allows the identification of critical points, was also obtained, as shown in the following figures.

Table 4. Summary of the PVT collector configurations selected for the structural characterisation.

Copper	S&T_D8-n9	3×2 mm	
Aluminium	S&T_D8-n9	3×2 mm	
PC	3×2 mm	6×4 mm	10×10 mm
PA30-33	3×2 mm		

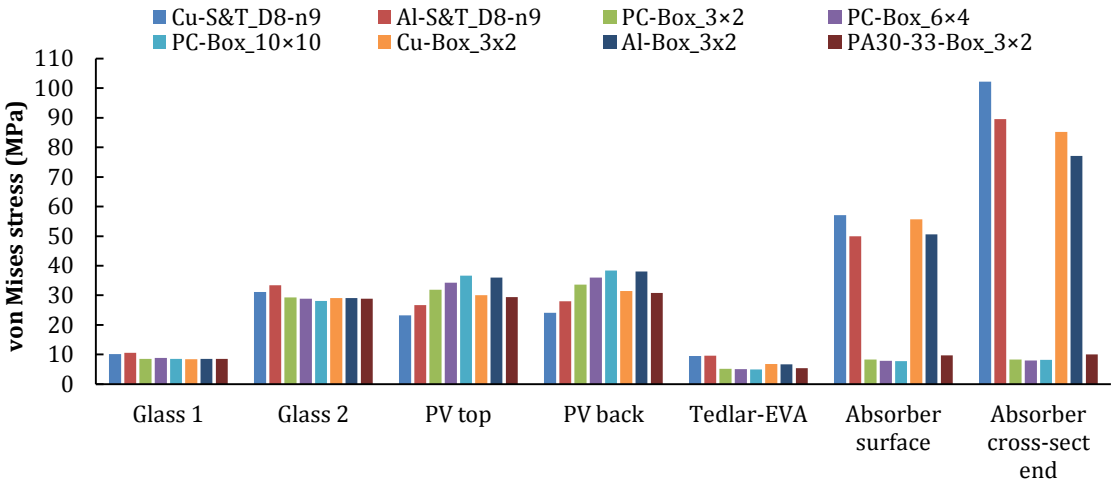

Figure 12. Maximum values of von Mises stress (MPa) for the different layers of the PVT configurations.

By comparing the von Mises stress in the different PVT layers with their corresponding yield or UTS, based on the most restrictive value for each particular case, it is possible to conclude that no yield or fracture is expected in any of the layers. For the cover and inner glasses (Glass 1 and Glass 2 respectively), the maximum von Mises stress is lower than 7% and 19% of the UTS, respectively (see Figure 12 and Table 1). In terms of stress distribution throughout the layers' surfaces, the results show that in all PVT collector configurations, the maximum von Mises stress for Glass 1 occurs at the collector water inlet (see Figure 13 top), which is attributed to its weight effect at the tilted angle. Meanwhile, the maximum value for Glass 2 occurs at the end of the collector, where the maximum thermal expansion occurs, as it is where the higher temperatures are achieved (see Figure 13 bottom).

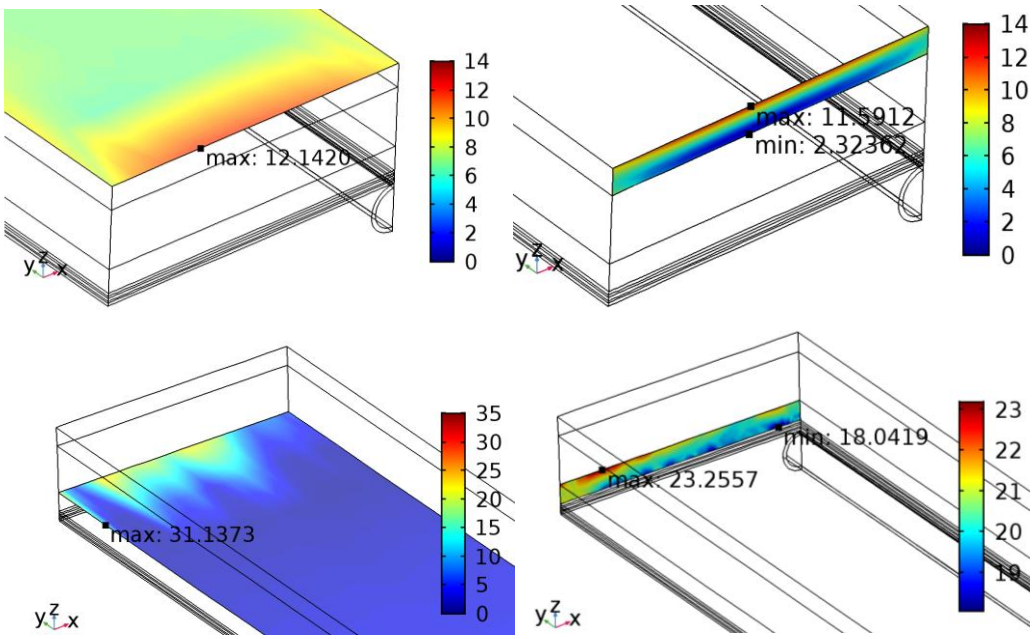

Figure 13. (Top) Von Mises Stress (MPa) for Glass 1 in the (left) upper part, and (right) cross-sectional area at the collector water inlet; (bottom) Von Mises Stress (MPa) for Glass 2 in the (left) upper part, and (right) cross-sectional area at the collector outlet, for the sheet-and-tube copper PVT collector.

The maximum von Mises stress in the PV layer is between 14% to 23% of its UTS, with the PC 10×10 mm flat-box design experiencing the highest stress due to a greater thermal expansion suffered in the *z*-direction. It is observed that for the polymeric (PC and PA30-33) flat-box designs, the layer that suffers the highest strains is the PV module, with higher von Mises stress values than for the sheet-and-tube PVT collector (see Figure 12). This is attributed to the larger buckling of the former configurations, especially in the *z*-direction, as shown in

Figure 14 right. Specifically, the critical point occurs in a section towards the collector fluid outlet as indicated in Figure 14 (left). It should be noted that the PV layer buckling is the same as for the whole PVT collector since all layers are assumed to be maintained in contact (except for Glass 1) (see Figure 14 right).

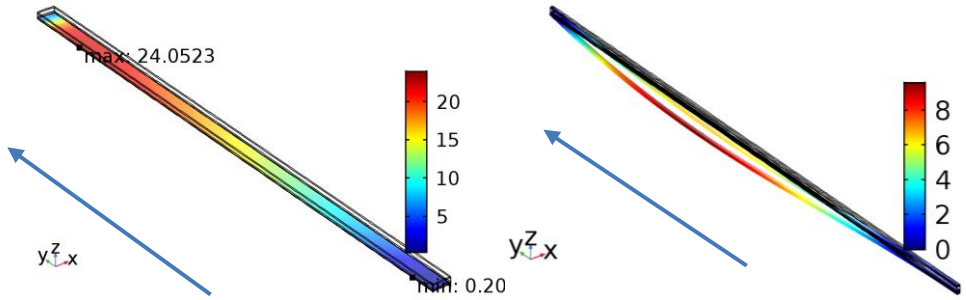

Figure 14. Von Mises Stress (MPa) of the PV layer (left) and thermal expansion of the PVT collector in the z-direction (mm) (right) throughout its length for the PC 3×2 mm PVT collector. Blue arrow shows the flow direction.

Regarding the variation of the strains for the PC flat-box configurations with different channel dimensions, Figure 12 shows that the von Mises stress increases with the channel dimensions. The thermal expansion that the PVT collector suffers, defined as displacement divided by the total collector length, in percentage, increases as well with channel dimensions, from 0.6% to 0.8% displacement in the *z*-direction with respect to the total length, and from 0.04% to 0.07% in the *y*-direction)

Finally, concerning the absorber-exchanger, the most critical configuration in terms of strains suffered is the sheet-and-tube collector, in which the maximum von Mises stress is around 64% and 56% of the yield stress for the copper and aluminium configurations respectively. The maximum stress occurs in the bonding between the absorber layer and the riser pipe at the collector water outlet. This result is expected since: i) this is the area where the highest temperatures are reached, and ii) stress is concentrated in a very small surface area compared with the rest of the PVT layers. As a consequence, the sheet-and-tube configuration is the one with the highest strains.

It should be noted that the values of the mechanical properties can vary within a wide range depending on the specific copper and aluminium alloys used for the bonding in each case, so more accurate values (provided by the sheet-and-tube collector manufacturer) are necessary for a more detailed structural analysis. In all of the absorber-exchanger flat-box designs, the maximum von Mises stress within the absorber-exchanger is located in the cross-sectional area at the collector outlet (see Figure 15), and amounts to <37% of the yield stress of the metal (copper, aluminium) collectors and <13% of the yield stress of the polymeric collectors. Additionally, as shown in Figure 12, the maximum overall collector strains in the copper and aluminium flat-box configurations occur in the aforementioned absorber-exchanger cross-sectional area at the collector water outlet, together with the maximum thermal expansion in the *y*-direction (see Figure 15).

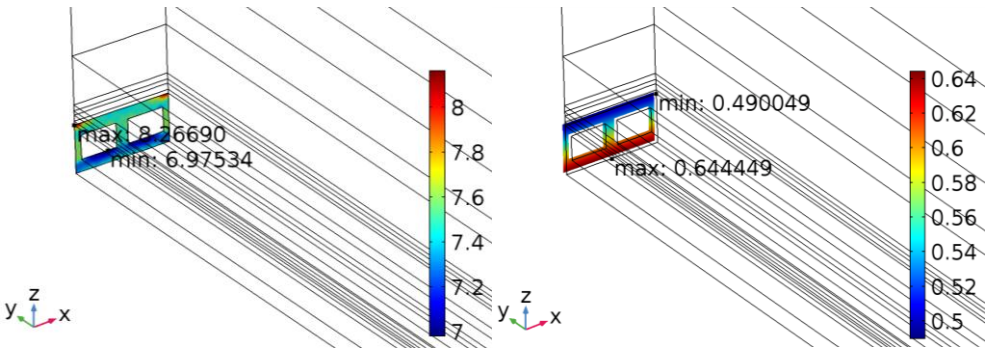

Figure 15. (left) Von Mises stress (MPa) and (right) thermal expansion in the y-direction (mm) over the cross-sectional area of the absorber-exchanger for the PC flat-box 3×2 mm configuration.

4.5 Technoeconomic analysis

Figure 16 compares the PVT collector designs proposed in this work to the reference PVT collector (Cu-S&T_D8-n9), reporting percentage relative improvements relative to the latter. Positive improvements correspond to an increase in thermal efficiency (η_{th}), electrical efficiency (η_e) or heat removal factor (F_R), and to a reduction in the heat-loss coefficient (U_L) or payback time (*PBT*). Of the different copper sheet-and-tube designs, the largest thermal and electrical efficiency improvements (by 2.3% and 1.7%, respectively) are obtained for the n = 18 (D = 8 mm) case, although this design has a higher *PBT* (by 2.6%) than the reference case (with n = 9), resulting in a negative *PBT* improvement value in Figure 16. An intermediate case is the collector with 12 riser tubes (D = 8 mm), with more modest thermal and electrical efficiency improvements (1.1% and 0.8%, respectively), but with almost no increase in the *PBT*. This suggests that the higher PVT collector price due to larger number of tubes is compensated, to a certain extent, by the increased cost savings achieved by this collector, thanks to the improved heat recovery.

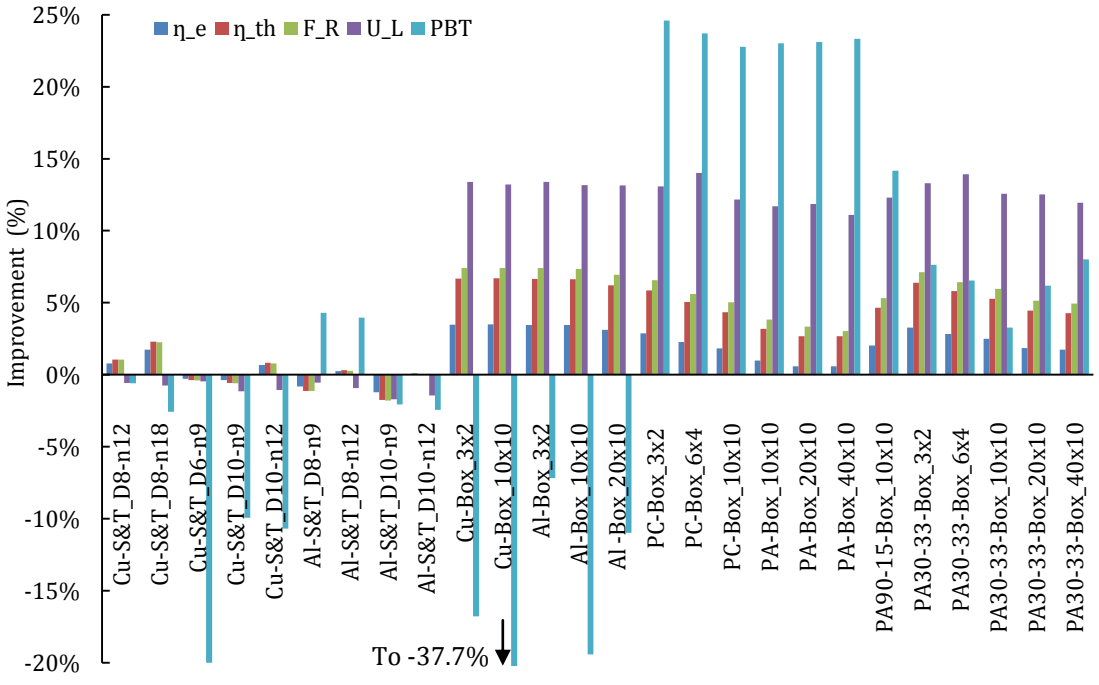

Figure 16. Percentage of improvement of the electrical (η_e) and thermal (η_{th}) efficiency, heat removal factor, (F_R), overall heat-loss coefficient (U_L) and payback time (PBT) of the different PVT designs studied compared to the reference PVT collector (Cu-S&T_D8-n9).

Turning to the aluminium sheet-and-tube collectors, the reference design (Al-S&T_D8-n9) has a slightly lower electrical (-0.8%) and thermal (-1.1%) performance than the equivalent copper reference collector, due to the marginally higher (0.5%) overall heat-loss coefficient (U_L) and lower (1.1%) heat removal factor (F_R), but its lower investment cost (-5%) leads to a shorter *PBT* (4.3% lower than the reference case). As with the copper collectors discussed above, the aluminium sheet-and-tube collector with 12 riser tubes (D = 8 mm) performs the best, also with 4% lower *PBT* and 11.7% less weight than the reference collector, so it can be concluded that this design is a good alternative for decreasing the weight and cost of the PVT collector while maintaining the electrical efficiency and slightly increasing the thermal efficiency.

Figure 16 shows that all the flat-box designs outperform the reference PVT collector, with higher electrical (0.6-3.5%) and thermal (2.7-6.7%) efficiencies, as more heat can be extracted thanks to the higher heat transfer area of the channels. This also leads to higher (3.0-7.4%) F_R and lower (11.1-14.0%) U_L. Among them, the PA absorber-exchanger designs perform the worst, as PA has the lowest thermal conductivity (see Table 1), while the copper and aluminium flat-box designs perform the best, as expected. In terms of channel dimensions, it is observed that the electrical and thermal efficiencies increase as the channel dimensions decrease, as more heat can be extracted, also leading to lower overall heat-loss coefficients

(see Figure 16). When bringing costs into consideration, the results show that all flat-box designs have a lower *PBT* than the reference PVT collector (up to 24.6% lower), except for the copper and aluminium flat-box designs which have up to 37.7% higher *PBT*, due to the significantly higher PVT collector cost. This can be clearly observed in Figure 17, where the copper and aluminium flat-box designs (blue squares and dark blue crosses respectively) considerably differ from the rest of the data. The higher PVT collector costs of these designs compared to the other alternatives is attributed to two main factors: i) the increased amount of required construction material for the flat-box structure than for the sheet-and-tube configuration, and ii) the higher cost of copper and aluminium than that of polymer, which are not outweighed by the higher cost savings.

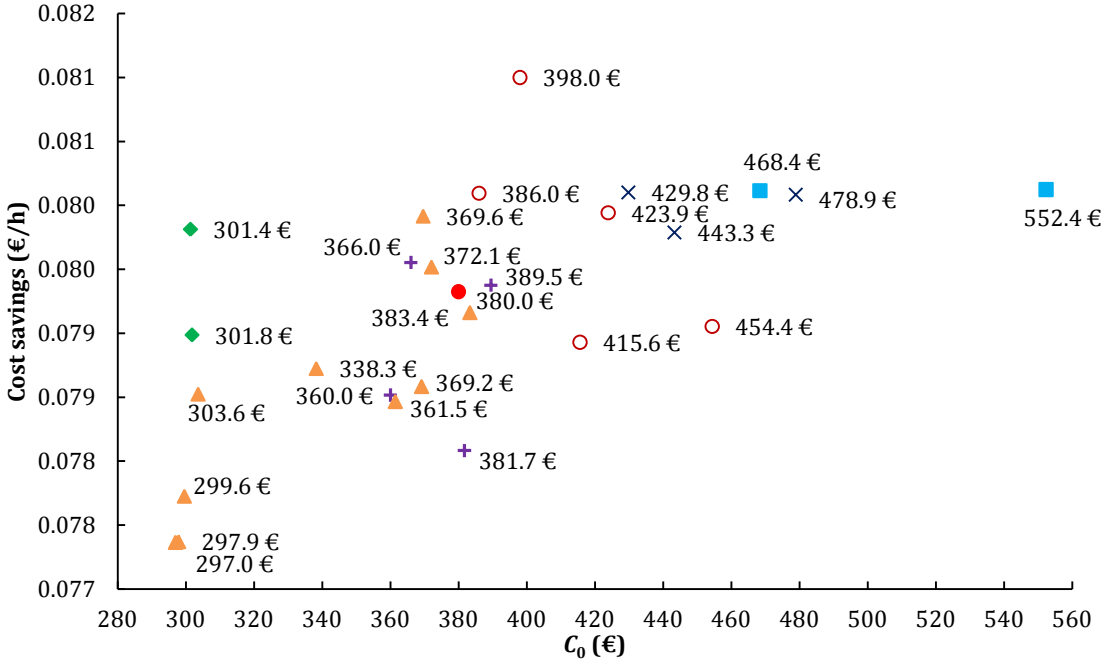

Figure 17. Cost savings (€/h) vs. PVT collector cost for the different designs studied. Results of the flat-box designs reproduced from previous work [59]. *(Red circle = reference case, unfilled circles= copper S&T, purple pluses = Aluminium S&T, blue squares = copper flat-box, dark blue crosses = aluminium flat-box, green diamonds = PC 3×2 mm and 6×4 mm flat-box designs, orange triangles = rest of polymeric flat-box).*

The results for the copper sheet-and-tube designs show that all such designs (unfilled circles) are worse than the reference case except the Cu-S&T_D8-n12 (C_0 = 386.0 €) and Cu-S&T_D8-n18 (C_0 = 398.0 €) collector designs, which corroborates the previous observations. From the aluminium sheet-and-tube collectors (purple pluses), the Al-S&T_D8-n12 design (C_0 = 366.0 €) appears as a promising alternative to the reference case, with lower PVT collector cost and slightly higher cost savings.

Considering the polymeric flat-box designs, the worst results are found for the PA with higher loading of additives (PA30-33) due to the high cost of the additive (orange triangles above and below the reference collector), but still the designs with smaller channels (3×2 mm and 6×4 mm) have higher cost savings than the reference collector. Conversely, the lowest collector costs are when using PC and PA without additives, as expected, due to the lower cost of the raw material (orange triangles appearing on the left of Figure 17). From these, the best results are obtained for the PC flat-box design, in particular the 3×2 mm and 6×4 mm (upper and lower green diamonds, respectively) with which high cost savings are achieved, compared to the rest of the channel designs. Thus, the PC-box-3×2 and PC-box-6×4 collector designs appear as the most promising alternatives, with 24.6% and 23.7% lower *PBT*, and 8.7% and 8.5% lower weight respectively, relative to the reference case collector.

5. Further Discussion and Conclusions

Previous research [6,7,13] showed that PVT-w systems have an important role to play in urban energy system decarbonisation roadmaps. Nevertheless, and even though hybrid PVT collectors are a commercially mature technology already available on the market, their uptake remains limited by high costs compared to PV-only systems [14], as well as a lack of knowledge in this technology. Therefore, as previous studies have concluded [1], more research is required to develop new high-efficiency yet affordable PVT systems, and to promote their commercial acceptance.

The motivation of the present research was to investigate the potential of improved hybrid PVT collectors with an optimal balance of performance, weight, cost and ease of manufacture. To this end, new absorber-exchanger configurations were considered based on geometrical designs and polymer construction materials that achieve significant reductions in weight and cost relative to conventional copper sheet-to-tube designs, while improving or at least maintaining the overall (thermal + electrical) efficiency of the collectors.

Specifically, 18 different flat-box designs and 9 alternative sheet-and-tube designs for the absorber-exchanger (plus a benchmark reference case) were analysed in order to assess and compare their performance. For each of these designs, a 3-D model was developed in FEM and CFD software (COMSOL), which was then used to obtain their corresponding characteristic curves and identify the design parameters that optimise their performance. The 3-D model was validated against a manufacturer's performance curve and a grid independence mesh convergence study was undertaken in COMSOL. In addition, a simple cost analysis was undertaken to compare the designs from a cost perspective.

The analysis performed for the copper sheet-and-tube (Cu-S&T) collectors showed that the pipe diameter does not have an important effect on the thermal efficiency of the collector, whereas an increase in the number of riser tubes significantly improves its thermal and electrical efficiencies up to about 20-25 pipes, beyond which both efficiencies approach an asymptote. However, when considering the investment costs and costs savings of these collectors, it was observed that Cu-S&T collectors with more riser pipes have higher payback periods due to their high investment costs, which is not outweighed by their slightly better performance (up to 2.3% relative) higher thermal efficiency for n = 18 compared to the reference n = 9).

Similar results were obtained for the aluminium sheet-and-tube (Al-S&T) collectors, although in this case the lower material cost allows lower investment costs that outweighed the slightly worse thermal performance of the absorber-exchanger caused by the lower thermal conductivity of aluminium. Therefore, the Al-S&T_D8-n12 design is considered an interesting alternative to the reference case, as it maintains the electrical/thermal efficiencies while reducing both the investment cost (by 3.7%) and the weight (by 11.7%) of the collector.

All flat-box designs outperformed the reference PVT collector (Cu-S&T_D8-n9), due to the increased heat transfer area between the absorber and the fluid. Furthermore, with the proposed flat-box designs, the temperature distribution over the PV surface is more uniform, which alleviates the appearance of hot spots and leads to lower PV cell temperatures, e.g., compared to those observed in-between pipes in the S&T design. As a consequence, although the thermal conductivity of the considered polymers is lower than that of copper, all of the flat-box designs achieve a higher (up to 4.8%) optical efficiency (η_o) and a lower (up to 15.7%) heat-loss coefficient (a_1) compared to the reference collector.

Furthermore, it is observed that for the same channel dimensions, the solid construction material does not have a significant influence on the collector's thermal performance, with a variation of less than 5% between the performance curves of the best (copper) and worst (PA) collectors, due to the fact that this is not the dominant thermal resistance in the collector. Similarly, the best results are found for the flat-box design with the smallest (3×2 mm) channel dimensions and the worst for the largest (40×10 mm) channel dimensions, although the channel dimensions (for the same material) only weakly affect the collector's thermal efficiency. This is attributed to the nearly 7 times higher heat transfer coefficient of the water flowing through the smallest channels. Therefore, it can be concluded that the critical factor in achieving a good thermal and electrical performance in the type of investigated PVT-w collectors is to maximise the heat transfer area rather than minimise the thermal resistance, thereby extracting the maximum amount of

heat from the absorber-exchanger. It should be noted that the proposed designs have a thin absorber plate (1 mm) and low fluid velocities (resulting in laminar flows with $Re < 250$). Thus, the effect of varying the materials and channel dimensions on the PVT collector performance, while observable, is small and not considered significant within the operational range proposed in this study.

To complement the thermal (and economic) aspects of this study, a conservative structural analysis was performed on the developed and validated 3-D FEM and CFD thermal-fluid model for the most promising and representative PVT collector designs. The results show that the PVT flat-box designs proposed in this research appear as a very promising alternative to the reference (Cu-S&T) collector, since apart from the aforementioned improvements: i) in general, the maximum von Mises stresses suffered by the different PVT layers in the flat-box designs are lower than for the S&T collector, e.g., in the absorber-exchanger, which is the layer suffering more stresses in the S&T designs, the maximum von Mises stress is <13% *vs*. 64% of the yield stress in the polymeric flat-box *vs*. the copper S&T collectors; furthermore, ii) even though the buckling suffered by the flat-box designs is higher (up to around 90% higher in the worst case, PC 10×10 mm configuration), the displacement in the *z*-direction (vertical) is only 0.8% with respect to the total length in that case. Therefore, these flat-box designs are not expected to suffer higher strains than the commercially available PVT collectors, but they are expected to achieve higher thermal efficiencies at lower investment costs, thus lower payback periods.

Finally, an economic analysis reveals that the slightly better thermal and electrical performance of the copper and aluminium flat-box designs does not compensate their significantly higher investment costs (due to the higher material costs compared to those of the polymers). Among the various polymeric absorber-exchanger alternatives studied, it was also found that the loading of these polymers with additives in order to increase their thermal conductivity considerably increases the PVT collector cost, while only achieving marginal cost savings (once again in line with the above observations relating to the role of the thermal resistance). Consequently, it can be concluded that flat-box designs from off-the-shelf polymers are a promising alternative to commercial PVT collectors, without additive loading. These configurations can achieve an improvement in the thermal and electrical performance of the PVT collector, while lowering the investment cost (by up to 22%) and weight (up to 10%) of the PVT collector. Specifically, the results show that the PC 3×2 mm flat-box design achieves the lowest payback period (24.6% lower than the reference collector) due to the lower investment cost (21% lower) and better energy performance, 5.9% and 2.9% (relative) higher thermal and electrical efficiencies respectively, than the reference (Cu-S&T) collector. This design also leads to a 9% reduction in the total PVT collector weight, which implies a promising reduction in the energy consumption and costs associated with the PVT collector manufacture, transport and installation. Even though transport, installation and other related costs have not been considered in the present research, these issues are of importance, together with the life cycle environmental impact of the different proposed materials, recyclability, raw materials required for the manufacturing process, etc. Therefore, a life cycle environmental impact assessment is proposed as further work to fully characterise the proposed novel design from a performance, economic and environmental perspective. In addition, further work is also required to: i) analyse in detail the structural and energy performance of the whole PVT collector in the 3-D FEM and CFD model, to consider also the effect of the sides of the PVT collector (both in terms of energy losses and structural analysis), ii) manufacture a prototype of the proposed PVT collector design and undertake experimental analysis to assess its real performance, iii) assess the energy performance of a complete PVT-based solar combined heat and power (S-CHP) system throughout the whole year, and iv) assess and optimise the S-CHP system parameters (such as PVT collector flow-rate, number of PVT collectors, water tank size, etc.) when installed in a building to maximise the percentage of energy demand covered throughout a year.

Acknowledgements

This work was undertaken as part of the PhD Programme 'Renewable Energies and Energy Efficiency' of the University of Zaragoza – CIRCE Research Institute, during the international placement of MH at Imperial College London that was partially funded by the University of Zaragoza, Fundación Bancaria

Ibercaja and Fundación CAI under the CAI-Ibercaja Program of Research Placements [reference number IT9/16]. This work was also supported by the UK Engineering and Physical Sciences Research Council (EPSRC) [grant number EP/M025012/1]. The technical specifications and some experimental results relating to the commercially available ECOMESH panel were provided by the PVT collector manufacturer, EndeF Engineering. Part of this work was presented at the ISES EuroSun 2016 Conference. Data supporting this publication can be obtained on request from cep-lab@imperial.ac.uk.

References

[1] Michael JJ, Iniyan S, Goic R. Flat plate solar photovoltaic-thermal (PV/T) systems: A reference guide. Renew Sustain Energy Rev 2015;51:62–88. doi:10.1016/j.rser.2015.06.022.

[2] Zondag HA. Flat-plate PV-Thermal collectors and systems: A review. Renew Sustain Energy Rev 2008;12:891–959. doi:10.1016/j.rser.2005.12.012.

[3] Allan J, Dehouche Z, Stankovic S, Mauricette L. Performance testing of thermal and photovoltaic thermal solar collectors. Energy Sci Eng 2015;3:310–26. doi:10.1002/ese3.75.

[4] Santbergen R, van Zolingen RJC. The absorption factor of crystalline silicon PV cells: A numerical and experimental study. Sol Energy Mater Sol Cells 2008;92:432–44. doi:10.1016/j.solmat.2007.10.005.

[5] Dupeyrat P, Ménézo C, Fortuin S. Study of the thermal and electrical performances of PVT solar hot water system. Energy Build 2014;68:751–5. doi:10.1016/j.enbuild.2012.09.032.

[6] Herrando M, Markides CN, Hellgardt K. A UK-based assessment of hybrid PV and solar-thermal systems for domestic heating and power: System performance. Appl Energy 2014;122:288–309. doi:10.1016/j.apenergy.2014.01.061.

[7] Antonanzas J, del Amo A, Martinez-Gracia A, Bayod-Rujula AA, Antonanzas-Torres F. Towards the optimization of convective losses in photovoltaic–thermal panels. Sol Energy 2015;116:323–36. doi:10.1016/j.solener.2015.04.013.

[8] Fudholi A, Sopian K, Yazdi MH, Ruslan MH, Ibrahim A, Kazem HA. Performance analysis of photovoltaic thermal (PVT) water collectors. Energy Convers Manag 2014;78:641–51. doi:10.1016/j.enconman.2013.11.017.

[9] Hansen J, Sorensen H, Byström J, Collins M, Karlsson B. Market, Modelling, Testing and Demonstration in the Framework of IEA SHC Task 35 on PV/Thermal Solar Systems. IEA 2007;83:199–210.

[10] Affolter P, Eisenmann W, Fechner H, Rommel M, Schaap A, Sorensen H, et al. PVT roadmap: A European guide for the development and market introduction of PV-Thermal technology. 20th European Photovoltaic Solar Energy Conference and Exhibition 2005.

[11] Kempener R, Burch J, Navntoft C, Mugnier D, Nielsen JE, Weiss W. Solar Heating and Cooling for Residential Applications. IEA-ETSAP and IRENA 2015.

[12] Guarracino I, Mellor A, Ekins-Daukes NJ, Markides CN. Dynamic coupled thermal-and-electrical modelling of sheet-and-tube hybrid photovoltaic / thermal (PVT) collectors. Appl Therm Eng 2016;101:778–95. doi:10.1016/j.applthermaleng.2016.02.056.

[13] Guarracino I, Freeman J, Ekins-Daukes N, Markides CN. Performance assessment and comparison of solar ORC and hybrid PVT systems for the combined distributed generation of domestic heat and power. International Conference on Heat Transfer, Fluid Mechanics and Thermodynamics, 2016.

[14] Herrando M, Markides CN. Hybrid PV and solar-thermal systems for domestic heat and power provision in the UK: Techno-economic considerations. Appl Energy 2016;161:512–32. doi:10.1016/j.apenergy.2015.09.025.

[15] Zhang X, Zhao X, Smith S, Xu J, Yu X. Review of R&D progress and practical application of the solar photovoltaic/thermal (PV/T) technologies. Renew Sustain Energy Rev 2012;16:599–617. doi:10.1016/j.rser.2011.08.026.

[16] IEA. Technology Roadmap: Solar Heating and Cooling. Paris (France), 2012.

[17] International Energy Agency. Task 60: PVT Systems: Application of PVT Collectors and New Solutions in HVAC Systems, 2018.

[18] Cuddihy EF, Coulbert CD, Willis P, Baum B, Garcia A, Minning C. Polymeric Encapsulation Materials for Low-Cost, Terrestrial, Photovoltaic Modules. Polym Sol Energy Util 1983;220;22–353. doi:10.1021/bk-1983-0220.ch022.

[19] Rosenthal AL, Thomas MG, Durand SJ. A ten year review of performance of photovoltaic systems. 23rd IEEE Photovoltaic Specialists Conference, 1993:1289–91. doi:10.1109/PVSC.1993.346934.

[20] Czanderna AW, Pern FJ. Encapsulation of PV modules using ethylene vinyl acetate copolymer as a pottant: A critical review. Sol Energy Mater Sol Cells 1996;43:101–81. doi:10.1016/0927-0248(95)00150-6.

[21] Magalhães PMLP, Martins JFA, Joyce ALM. Comparative Analysis of Overheating Prevention and Stagnation Handling Measures for Photovoltaic-thermal (PV-T) Systems. Energy Procedia 2016;91:346–55. doi:10.1016/j.egypro.2016.06.282.

[22] Zondag HA, van Helden WGJ. Stagnation Temperature in PVT Collectors, 2002.

[23] Fischer J, Bradler PR, Schlaeger M, Wallner GM, Lang RW. Novel Solar Thermal Collector Systems in Polymer Design - Part 5: Fatigue Characterization of Engineering PA Grades for Pressurized Integrated Storage Collectors. Energy Procedia 2016;91:392–402. doi:10.1016/j.egypro.2016.06.167.

[24] Fortuin S, Hermann M, Stryi-Hipp G, Nitz P, Platzer W. Hybrid PV-Thermal collector development: Concepts, experiences, results and research needs. Energy Procedia 2014;48:37–47. doi:10.1016/j.egypro.2014.02.006.

[25] Magalhães PMLP, Martins JFA, Joyce ALM. Performance Assessment of Tank Fluid Purging and Night Cooling as Overheating Prevention Techniques for Photovoltaic-Thermal (PV-T) Solar Water Heating Systems. IFIP Int. Fed. Inf. Process. 2017;499;337–347. doi:10.1007/978-3-319-56077-9.

[26] Ramschak T, Hausner R, Fink C. Polymeric Materials in Solar-thermal Systems - Performance Requirements and Loads. Energy Procedia 2016;91:105–12. doi:10.1016/j.egypro.2016.06.182.

[27] Martinopoulos G, Missirlis D, Tsilingiridis G, Yakinthos K, Kyriakis N. CFD modeling of a polymer solar collector. Renew Energy 2010;35:1499–508. doi:10.1016/j.renene.2010.01.004.

[28] Tagliafico LA, Scarpa F, De Rosa M. Dynamic thermal models and CFD analysis for flat-plate thermal solar collectors – A review. Renew Sustain Energy Rev 2014;30:526–37. doi:10.1016/j.rser.2013.10.023.

[29] Selmi M, Al-Khawaja MJ, Marafia A. Validation of CFD simulation for flat plate solar energy collector. Renew Energy 2008;33:383–7. doi:10.1016/j.renene.2007.02.003.

[30] Marroquín-De Jesús Á, Olivares-Ramírez JM, Jiménez-Sandoval O, Zamora-Antuñano MA, Encinas-Oropesa A. Analysis of Flow and Heat Transfer in a Flat Solar Collector with Rectangular and Cylindrical Geometry Using CFD. Ing Investig Tecnol 2013;14:553–61. doi:10.1016/S1405-7743(13)72265-0.

[31] Henderson D, Junaidi H, Muneer T, Grassie T, Currie J. Experimental and CFD investigation of an ICSSWH at various inclinations. Renew Sustain Energy Rev 2007;11:1087–116. doi:10.1016/j.rser.2005.11.003.

[32] Singh Yadav A, Bhagoria JL. Heat transfer and fluid flow analysis of solar air heater: A review of CFD approach. Renew Sustain Energy Rev 2013;23:60–79. doi:10.1016/j.rser.2013.02.035.

[33] Corbin CD, Zhai ZJ. Experimental and numerical investigation on thermal and electrical performance of a building integrated photovoltaic-thermal collector system. Energy Build 2010;42:76–82. doi:10.1016/j.enbuild.2009.07.013.

[34] Moreno D, Fernandez M, Esquivias PM. A comparison of closed-form and finite-element solutions for heat transfer in a nearly horizontal, unglazed flat plate PVT water collector: Performance assessment. Sol Energy 2017;141:11–24. doi:10.1016/j.solener.2016.11.015.

[35] Makki A, Omer S, Sabir H. Advancements in hybrid photovoltaic systems for enhanced solar cells performance. Renew Sustain Energy Rev 2015;41:658–84. doi:10.1016/j.rser.2014.08.069.

[36] Daghigh R, Ruslan MH, Sopian K. Advances in liquid based photovoltaic/thermal (PV/T) collectors. Renew Sustain Energy Rev 2011;15:4156–70. doi:10.1016/j.rser.2011.07.028.

[37] Chow TT. A review on photovoltaic / thermal hybrid solar technology. Appl Energy 2010;87:365–79. doi:10.1016/j.apenergy.2009.06.037.

[38] Chow TT, Ji J, He W. Photovoltaic-Thermal Collector System for Domestic Application. J Sol Energy Eng 2007;129:205. doi:10.1115/1.2711474.

[39] Tripanagnostopoulos Y, Souliotis M, Battisti R, Corrado A. Energy, cost and LCA results of PV and hybrid PV/T solar systems. Prog Photovoltaics Res Appl 2005;13:235–50. doi:10.1002/pip.590.

[40] Zondag HA, de Vries DW, van Helden WGJ, van Zolingen RJC, van Steenhoven AA. The yield of different combined PV-thermal collector designs. Sol Energy 2003;74:253–69. doi:10.1016/S0038-092X(03)00121-X.

[41] Chow TT. Performance analysis of photovoltaic-thermal collector by explicit dynamic model. Sol Energy 2003;75:143–52. doi:10.1016/j.solener.2003.07.001.

[42] Kalogirou SA. Use of TRNSYS for modelling and simulation of a hybrid PV–Thermal solar system for Cyprus. Renew Energy 2001;23:247–60. doi:10.1016/S0960-1481(00)00176-2.

[43] del Amo A, Martínez-Gracia A, Bayod-Rújula AA, Antoñanzas J. An innovative urban energy system constituted by a photovoltaic/thermal hybrid solar installation: Design, simulation and monitoring. Appl Energy 2016;186;140-151. doi:10.1016/j.apenergy.2016.07.011.

[44] EndeF Engineering. Technical Datasheet ECOMESH panel 2017.

[45] Ji J, Han J, Chow TT, Yi H, Lu J, He W, et al. Effect of fluid flow and packing factor on energy performance of a wall-mounted hybrid photovoltaic/water-heating collector system. Energy Build 2006;38:1380–7. doi:10.1016/j.enbuild.2006.02.010.

[46] Chow TT, Chan ALS, Fong KF, Lin Z, He W, Ji J. Annual performance of building-integrated photovoltaic/water-heating system for warm climate application. Appl Energy 2009;86:689–96. doi:10.1016/j.apenergy.2008.09.014.

[47] Cristofari C, Notton G, Canaletti JL. Thermal behavior of a copolymer PV/Th solar system in low flow rate conditions. Sol Energy 2009;83:1123–38. doi:10.1016/j.solener.2009.01.008.

[48] Cristofari C, Notton G, Poggi P, Louche A. Modelling and performance of a copolymer solar water heating collector. Sol Energy 2002;72:99–112. doi:10.1016/S0038-092X(01)00092-5.

[49] Cristofari C, Canaletti J, Notton G, Darras C. Innovative patented PV/TH Solar Collector: optimization and performance evaluation. Energy Procedia 2012;14:235–40.

[50] Huang BJ, Lin TH, Hung WC, Sun FS. Performance evaluation of solar photovoltaic / thermal systems. Sol Energy 2001;70:443–8.

[51] Ghaffari Mosanenzadeh S, Liu MW, Osia A, Naguib HE. Thermal Composites of Biobased Polyamide with Boron Nitride Micro Networks. J Polym Environ 2015;23:566–79. doi:10.1007/s10924-015-0733-8.

[52] European committee for Standardisation. European Standard EN 12975-2, in, CEN, 2006.

[53] Notton G, Cristofari C, Mattei M, Poggi P. Modelling of a double-glass photovoltaic module using finite differences. Appl Therm Eng 2005;25:2854–77. doi:10.1016/j.applthermaleng.2005.02.008.

[54] Agarwal RK, Garg HP. Study of a Photovoltaic-Thermal system - Thermosyphonic solar water heater combined with solar cells. Energy Convers Manag 1994;35:605–20.

[55] Bhattarai S, Oh J, Euh S, Krishna G, Hyun D. Simulation and model validation of sheet and tube type photovoltaic thermal solar system and conventional solar collecting system in transient states. Sol Energy Mater Sol Cells 2012;103:184–93. doi:10.1016/j.solmat.2012.04.017.

[56] Sandnes B, Rekstad J. A photovoltaic/thermal (PV/T) collector with a polymer absorber plate. Experimental study and analytical model. Sol Energy 2002;72:63–73. doi:10.1016/S0038-092X(01)00091-3.

[57] Zondag HA, De Vries DW, Van Helden WGJ, Van Zolingen RJC, van Steenhoven AA. The thermal and electrical yield of a PV-thermal collector. Sol Energy 2002;72:113–28. doi:10.1016/S0038-092X(01)00094-9.

[58] Tiwari A, Sodha MS. Performance evaluation of solar PV/T system: An experimental validation. Sol Energy 2006;80:751–9. doi:10.1016/j.solener.2005.07.006.

[59] Herrando M, Guarracino I, del Amo A, Zabalza I, Markides CN. Energy Characterization and Optimization of New Heat Recovery Configurations in Hybrid PVT Systems. ISES Conference Proceedings, Eurosun 2016, Palma de Mallorca (Spain). doi:10.18086/eurosun.2016.08.22.

[60] ASHRAE Standard. Standard 93-2003: Methods of testing to determine the performance of solar collectors. 2013.

[61] ISO 9806:2013 (e) Solar energy - solar thermal collectors - test methods, 2013.

[62] Collins M, Zondag HA. Recommended standard for the characterization and monitoring of PV/Thermal systems. Report DB2, 2009.

[63] Vokas G, Christandonis N, Skittides F. Hybrid photovoltaic – thermal systems for domestic heating and cooling — A theoretical approach. Sol Energy 2006;80:607–15. doi:10.1016/j.solener.2005.03.011.

[64] Skoplaki E, Palyvos JA. On the temperature dependence of photovoltaic module electrical performance: A review of efficiency/power correlations. Sol Energy 2009;83:614–24. doi:10.1016/j.solener.2008.10.008.

[65] Chow TT, He W, Ji J. Hybrid photovoltaic-thermosyphon water heating system for residential application. Sol Energy 2006;80:298–306. doi:10.1016/j.solener.2005.02.003.

[66] He W, Chow T, Ji J, Lu J, Pei G. Hybrid photovoltaic and thermal solar-collector designed for natural circulation of water. Appl Energy 2006;83:199–210. doi:10.1016/j.apenergy.2005.02.007.

[67] MakeItFrom.com. Toughened (Tempered) Soda-Lime Glass. http://www.makeitfrom.com/material-properties/Toughened-Tempered-Soda-Lime-Glass (accessed 7/02/2017).

[68] EndeF Engineering. EVASAFE DataSheet, 2017.

[69] GoodFellow. Tedlar - Polyvinylfluoride (PVF). http://www.findtheneedle.co.uk/companies/goodfellow-cambridge-ltd/products/tedlar-polyvinylfluoride-pvf (accessed 6/12/2016).

[70] Cambridge University Engineering Department. Materials data book. Mater Courses 2003:1–41. doi:10.1016/0261-3069(88)90026-X.

[71] Alanod Solar. Copper absorber plate, 2017.

[72] GoodFellow. Polycarbonate - online catalogue source - supplier of research materials in small quantities - Goodfellow. http://www.goodfellow.com/E/Polycarbonate.html (accessed 6/12/2016).

[73] Roylance D. Mechanical Properties of Materials. Springer 2008;190:645. doi:10.1007/978-94-007-4342-7.

[74] Von Mises R. Mechanik der Festen Korper im Plastisch Deformablen Zustand. Math Phys 1913;1:582–92.

[75] Hjelmstad KD. Fundamentals of Structural Mechanics. Second Edition. Urbana-Champaign, Illinois, Springer US; 2005.

[76] María Herrando, Ramos A, Zabalza I. Cost competitiveness of a novel PVT-based solar combined heating and power system: Influence of economic parameters and financial incentives. Energy Convers Manag 2018;166:758–70. doi:10.1016/j.enconman.2018.04.005.

[77] Preciogas. Natural gas price in Spain. http://preciogas.com/conceptos/precio-kwh (accessed 2/11/2016).

[78] Tarifaluzhora. Electricity price in Spain. http://tarifaluzhora.es/precio-electricidad-espana (accessed 2/11/2016).

[79] AITIIP. Technological Center. http://www.aitiip.com/ (accessed 1/12/2016).

[80] EndeF. Endef - Energy, Development and Future 2017. http://endef.com/ (accessed 10/02/2017).

[81] Alcaglas. Aluminum profile cut-to-size. http://www.alcaglas.com/infer.php?gr=perfiles-a-medida&sg=chapas-perfiles-aluminio (accessed 2/08/2016).

[82] Guarracino I, Freeman J, Markides CN. Experimental validation of a 3-D dynamic solar- thermal collector model under time-varying environmental conditions. 29th International Conference on Efficiency, Cost, Optimization, Simulation and Environmental Impact of Energy Systems, 2016.

[83] Ibrahim A, Othman MY, Ruslan MH, Alghoul MA, Yahya M, Zaharim A, et al. Performance of photovoltaic thermal collector (PVT) with different absorbers design. WSEAS Trans Environ Dev 2009;5:321–30.

[84] Ji J, Han J, Chow TT, Han C, Lu J, He W. Effect of flow channel dimensions on the performance of a box-frame photovoltaic/thermal collector. Proc Inst Mech Eng Part A-Journal Power Energy 2006;220:681–8. doi:10.1234/09576509jpe316.

[85] Bergene T, Lovvik OM. Model calculations on a flat-plate solar heat collector with integrated solar cells. Sol Energy 1995;55:453–62. doi:10.1016/0140-6701(96)88784-4.

[86] Kalogirou SA. Solar energy engineering: processes and systems. Second Edi. Academic Press; 2014. doi:10.1016/B978-0-12-374501-9.00014-5.

[87] Rejeb O, Dhaou H, Jemni A. Parameters effect analysis of a photovoltaic thermal collector: Case study for climatic conditions of Monastir, Tunisia. Energy Convers Manag 2015;89:409–19. doi:10.1016/j.enconman.2014.10.018.

[88] Lunde PJ. Solar thermal engineering: Space heating and hot water systems. John Wiley and Sons, 1980.

[89] Incropera FP, DeWitt DP, Bergman TL, Lavine AS. Fundamentals of Heat and Mass Transfer, Sixth Edit. John Wiley & Sons, 2007. doi:10.1016/j.applthermaleng.2011.03.022.

[90] Duffie JA, Beckman WA, Worek WM. Solar Engineering of Thermal Processes. John Wiley & Sons, 1974. doi:10.1115/1.2930068.

[91] Pierrick H, Christophe M, Leon G, Patrick D. Dynamic numerical model of a high efficiency PV-T collector integrated into a domestic hot water system. Sol Energy 2015;111:68–81. doi:10.1016/j.solener.2014.10.031.

[92] Hollands KGT, Unny TE, Raithby GD, Konicek L. Free convective heat transfer across inclined air layers. J Heat Transfer 1976;98:189–93.

[93] Cristofari C, Notton G, Poggi P, Louche A. Influence of the flow rate and the tank stratification degree on the performances of a solar flat-plate collector. Int J Therm Sci 2003;42:455–69. doi:10.1016/S1290-0729(02)00046-7.

[94] Anderson TN, Duke M, Morrison GL, Carson JK. Performance of a building integrated Photovoltaic/Thermal (BIPVT) solar collector. Sol Energy 2009;83:445–55. doi:10.1016/j.solener.2008.08.013.

Appendix A. PVT collector model equations

A.1 Glass cover energy balance

The top losses from the glass cover are mainly due to convection caused by wind, radiation from the top glass to the atmosphere and radiation from the PV layer to the atmosphere due to glass transmittance at long wavelengths [6,43,86],

$$q_{\text{top}} = q_{\text{wind}} + q_{\text{sky}} + q_{\text{rd,PVsky}} = h_{\text{cv,g1a}}\left(T_{\text{g1}} - T_{\text{a}}\right) + h_{\text{rd,g1sky}}\left(T_{\text{g1}} - T_{\text{sky}}\right) + h_{\text{rd,PVsky}}\left(T_{\text{PV}} - T_{\text{sky}}\right), \quad (7)$$

where q_{top} is the total heat loss to atmosphere, q_{wind} is the forced convective heat loss to the ambient wind, q_{sky} is the radiative heat flow from the glass cover to the atmosphere and $q_{\text{rd,PVsky}}$ is the radiative heat loss from the PV layer to the atmosphere at long wavelengths.

The heat flow through the glass cover and through the inert gas gap can be expressed as,

$$q_{\text{cd,g1}} = h_{\text{cd,g1}}\left(T_{\text{g1i}} - T_{\text{g1}}\right), \quad (8)$$

$$q_{\text{cd,g1}} = \left(h_{\text{cv,g1ig2}} + h_{\text{rd,g1ig2}}\right)\left(T_{\text{g2}} - T_{\text{g1i}}\right). \quad (9)$$

Now, each heat flux term is considered separately. All heat fluxes here are in W per unit area (W/m^2).

In order to model the convective heat exchange with the surroundings, the effect of the wind should be considered, and so a forced convective heat transfer coefficient is required [64]. Various expressions are given in different sources for the estimation of this coefficient [7,53,55,87,88], all of them dependent on the wind speed (v_{wind}). These expressions do not differ significantly, and so it was decided to use the expression that provides intermediate values, within the range of the various predictions [6]. Hence:

$$h_{\text{cv,g1ig2}} = 4.5 + 2.9v_{\text{wind}}. \quad (10)$$

The radiative heat loss to the atmosphere, q_{sky}, can be calculated from [89,90],

$$q_{\text{sky}} = \varepsilon_{\text{g,long}\lambda}\sigma\left(T_{\text{g1}}^4 - T_{\text{sky}}^4\right) = h_{\text{rd,g1ig2}}\left(T_{\text{g1}} - T_{\text{sky}}\right), \quad (11)$$

where $\varepsilon_{\text{g,long}\lambda}$ is the emissivity of the glass cover at long wavelengths, σ is the Stefan-Boltzmann constant ($\sigma = 5.67\cdot10^{-8}$ W/m^2 K^4), T_{g1} is the temperature of the glass cover, and T_{sky} is the sky temperature which can be found from the relation $T_{\text{sky}} = 0.0552T_{\text{a}}^{1.5}$ [6,47,53,90], with T_{a} in K. Therefore, the radiative term, also referred to as 'radiation heat transfer coefficient' can be expressed as [7,87],

$$h_{\text{rd,g1sky}} = \varepsilon_{\text{g,long}\lambda}\sigma\left(T_{\text{g1}}^2 + T_{\text{sky}}^2\right)\left(T_{\text{g1}} + T_{\text{sky}}\right). \quad (12)$$

The radiative heat loss from the PV layer to the atmosphere, $q_{\text{rd,PVsky}}$, accounts for the radiative heat flow emitted by the PV layer at long wavelengths that is not absorbed by the cover glass and therefore is lost to the atmosphere [90]. This term can be estimated considering the emissivity of the PV layer and the transmittance of the cover glass at long wavelengths as follows,

$$q_{\text{rd,PVsky}} = \tau_{\text{g,long}\lambda}\varepsilon_{\text{PV,long}\lambda}\sigma\left(T_{\text{PV}}^4 - T_{\text{sky}}^4\right) = h_{\text{rd,PVsky}}\left(T_{\text{PV}} - T_{\text{sky}}\right), \quad (13)$$

where $\tau_{\text{g,long}\lambda}$ is the transmittance of the cover glass and $\varepsilon_{\text{PV,long}\lambda}$ is the emissivity of the PV layer both at long wavelengths, and T_{PV} is the temperature of the PV layer. Thus, the radiative coefficient can be expressed as,

$$h_{\text{rd,PVsky}} = \tau_{\text{g,long}\lambda}\varepsilon_{\text{PV,long}\lambda}\sigma\left(T_{\text{PV}}^2 + T_{\text{sky}}^2\right)\left(T_{\text{PV}} + T_{\text{sky}}\right). \quad (14)$$

Conduction through the top glass depends on the glass thickness (δ_{g1}) and its thermal conductivity (k_{g1}),

$$h_{\mathrm{cd,g1}} = \frac{k_{\mathrm{g1}}}{\delta_{\mathrm{g1}}}. \tag{15}$$

As shown in Eq. (9), the heat flux through the inert gas gap is due to both convection and radiation. According to Ref. [90], the radiative heat transfer between two diffuse and infinity grey parallel plates of equal area at known temperatures, which is assumed here to be the case between the glass cover and the PV glass cover (with emissivity at long wavelengths $\varepsilon_{\mathrm{PV,long}\lambda}$), can be obtained from,

$$q_{\mathrm{rd,g1ig2}} = \sigma \frac{T_{\mathrm{g2}}^4 - T_{\mathrm{g1i}}^4}{1/\varepsilon_{\mathrm{PV,long}\lambda} + 1/\varepsilon_{\mathrm{g,long}\lambda} - 1}, \tag{16}$$

and thus, the radiation heat transfer coefficient between these layers can be expressed as [7,65,87],

$$h_{\mathrm{rd,g1ig2}} = \frac{\sigma\left(T_{\mathrm{g2}}^2 - T_{\mathrm{g1i}}^2\right)\left(T_{\mathrm{g2}} + T_{\mathrm{g1i}}\right)}{1/\varepsilon_{\mathrm{PV,long}\lambda} + 1/\varepsilon_{\mathrm{g,long}\lambda} - 1}. \tag{17}$$

Finally, the convective heat transfer coefficient between the glass cover and the PV glass cover can be estimated based on the estimation of a suitable Nusselt number (Nu),

$$h_{\mathrm{cv,g1ig2}} = \frac{Nu_{\mathrm{arg}} k_{\mathrm{arg}}}{\delta_{\mathrm{g1ig2}}}, \tag{18}$$

where Nu_{arg}, k_{arg} and δ_{g1ig2} represent the Nusselt number, the thermal conductivity of the inert gas encapsulated in the gap (Argon), and the distance between the glass cover and the PV glass cover. To estimate Nu_{arg},, several authors [7,65,86,87,91] have used an experimental equation proposed by Hollands et al. [92], as a function of the Rayleigh number (Ra) and tilt angle (β), valid for tilt angles from 0° to 60°,

$$Nu_{\mathrm{arg}} = 1 + 1.44\left[1 - \frac{1708}{Ra\cos\beta}\right]^{+} \cdot \left[1 - \frac{1708 \cdot (\sin 1.8\beta)^{1.6}}{Ra\cos\beta}\right] + \left[\left(\frac{Ra\cos\beta}{5830}\right)^{0.3} - 1\right]^{+}. \tag{19}$$

In this equation, Eq. (19), the notation $[\ldots]^{+}$ is used to indicate terms that are only considered if their value is positive. Rayleigh number (Ra) is given by,

$$Ra = \frac{g Pr_{\mathrm{arg}} \beta_{\mathrm{arg}} \left(T_{\mathrm{g2}} - T_{\mathrm{g1i}}\right) \delta_{\mathrm{g1ig2}}^3}{\upsilon_{\mathrm{arg}}^2}. \tag{20}$$

For titled surfaces, Ra < 1,700 means that the only heat transfer mechanism among the gas particles is conduction, whereas for Ra > 1,700 natural convection starts to appear.

A.2 PV layer energy balance

The calculation of the absorbed solar irradiance (S) is based on the ASHRAE convention [60], as used by several authors [53,56,86,93], which considers the three components of the incident radiation: beam (I_{b}), diffuse (I_{d}) and ground-reflected radiation, as follows,

$$S = (\tau\alpha)_{\mathrm{PV}} I_{\mathrm{t}} = (\tau\alpha)_{\mathrm{PV}} \left[R_{\mathrm{b}} I_{\mathrm{b}} K_{\mathrm{b}} + I_{\mathrm{d}} K_{\mathrm{d}} \frac{1 + \cos\beta}{2} + (I_{\mathrm{b}} + I_{\mathrm{d}}) \rho_{\mathrm{gro}} K_{\mathrm{gro}} \frac{1 - \cos\beta}{2}\right], \tag{21}$$

where $(\tau\alpha)_{\mathrm{PV}}$ is the transmittance-absorptance product for the PV module, which can be calculated as,

$$(\tau\alpha)_{\mathrm{PV}} = \frac{\tau_{\mathrm{g,short}\lambda} \alpha_{\mathrm{PV,short}\lambda}}{1 - \left(1 - \alpha_{\mathrm{PV,short}\lambda}\right)\rho_{\mathrm{d}}}, \tag{22}$$

following Ref. [90]. Here, $\tau_{g,short\lambda}$ is the transmittance of the cover plate (glass), $\alpha_{PV,short\lambda}$ is the absorptivity of the PV module, both at short wavelengths, and ρ_d is the diffuse reflectance of the cover plate. In the case of a single cover glass layer, as used in the present study, we employ a value of 0.16 for this parameter [90].

In Eq. (21), R_b is the ratio of beam radiation on the tilted surface to that on a horizontal surface, and can be estimated from the graphs available at Ref. [90], for a specific latitude (ϕ), tilted angle (β) and month. The incidence angle modifier for the direct component of solar radiation (K_b) is given by:

$$K_b = 1 + b_0\left(\frac{1}{\cos\theta_{eb}} - 1\right), \tag{23}$$

where θ_{eb} is the incidence angle of the beam solar radiation and can be estimated from graphs available in Ref. [90], for a specific latitude (ϕ), tilted azimuth (γ) and month; for single glazed collectors b_0 = -0.1 [53]. For the sky and ground diffuse radiation, the incidence angle modifiers (K_d, K_{gro}) are given as a function of the equivalent sky and diffuse incidence angles, which can be estimated following Ref. [90].

After neglecting the absorption of solar radiation by the top layer (glass cover) at short wavelengths, given the very low absorptivity of glass ($\alpha_{g,short\lambda}$ = 0.05), the global energy balance of the PVT collector is [6,7],

$$S = w_e + q_{top} + q_{cd,ca} \tag{24}$$

where w_e is the electrical yield of the system, which depends on the PV module efficiency. This term varies with temperature and can be estimated from [6,40,58,64],

$$w_e = I_t \tau_{g,short\lambda} \eta_{PV} \tag{25}$$

$$\eta_{PV} = \eta_{ref}[1 - \beta_0(T_{PV} - T_{ref})], \tag{26}$$

where η_{ref} is the reference module efficiency at a PV cell temperature, T_{ref}, of 25 °C and at a solar irradiance of 1,000 W/m^2 (value given by the manufacturer), and β_0 is the temperature coefficient for the PV module, also given in the technical specifications of the ECOMESH panel being considered.

Since a linear heat transmission was considered in this work, heat fluxes across layers (glass cover, inert gas gap, and PV glass cover) are equal. Therefore, Eqs. (7) and (8) are equal to,

$$q_{cd,g2} = h_{cd,g2}\left(T_{PV} - T_{g2}\right), \tag{27}$$

where $h_{cd,g2}$ is the equivalent heat transfer coefficient for conduction through the PV glass cover,

$$h_{cd,g2} = \frac{1}{\frac{\delta_{g2}}{k_{g2}} + \frac{\delta_{eva}}{k_{eva}}}. \tag{28}$$

Finally, the heat flow between the PV cells and the absorber ($q_{cd,ca}$) in Eq. (24) can be estimated as [6,40],

$$q_{cd,ca} = U_{bond}(T_{PV} - T_{abs}), \tag{29}$$

where T_{abs} is the temperature of the absorber plate, and U_{bond} is the heat transfer coefficient of the bonding, from the PV cell to the absorber plate, which is composed by the following layers: a pc-Si wafer, which has a very high thermal conductivity compared with the other layers (with $k \approx 149$ W/m K) and is therefore neglected, a 0.5 mm EVA layer (k = 0.35 W/m K) and a 0.3 mm thick Tedlar layer (k = 0.36 W/m K) [6,7],

$$U_{\text{bond}} = \frac{1}{\frac{\delta_{\text{eva}}}{k_{\text{eva}}} + \frac{\delta_{\text{tedlar}}}{k_{\text{tedlar}}}}. \quad (30)$$

A.3 Absorber-exchanger energy balance

The heat flow $q_{\text{cd,ca}}$ can be either transferred from the absorber layer to the cooling fluid (q_{u}), or lost through the underside insulation layer to the environment (q_{back}) [6,40],

$$q_{\text{cd,ca}} = q_{\text{u}} + q_{\text{back}}\,. \quad (31)$$

Here,

$$q_{\text{back}} = U_{\text{back}}(T_{\text{abs}} - T_{\text{a}})\,, \quad (32)$$

where T_{a} is the ambient temperature, and U_{back} is the heat transfer coefficient between the absorber and the environment (through the back-layer insulation), which can be calculated from,

$$U_{\text{back}} = \frac{1}{\frac{\delta_{\text{ins}}}{k_{\text{ins}}} + \frac{1}{h_{\text{cv,b}}}}, \quad (33)$$

where δ_{ins} and k_{ins} are the thickness and thermal conductivity of the insulation layer respectively, and $h_{\text{cv,b}}$ is the convective heat transfer coefficient of air at the back of the PVT module, which usually takes values between 0.3-0.6 W/m^2 K [86]; an average value of 0.45 W/m^2 K was considered in the present work [7].

The heat transfer from the absorber to the water, also called useful heat, q_{u}, is equal to the absorbed solar radiation minus the total heat losses from the surface to the surroundings by conduction, convection and radiation, which are represented by the product of the overall heat-loss coefficient, U_{L}, times the difference between the absorber plate temperature, T_{abs}, and the ambient temperature, T_{a}, as follows [86],

$$q_{\text{u}} = S - U_{\text{L}}(T_{\text{abs}} - T_{\text{a}})\,. \quad (34)$$

This term can also be estimated by [6,15],

$$q_{\text{u}} = \frac{\dot{m}_{\text{c}} c_{\text{p}} (T_{\text{out}} - T_{\text{in}})}{A_{\text{c}}}, \quad (35)$$

with $\dot{m}_{\text{c}}$ the mass flow-rate of water through the collector, c_{p} the specific heat capacity of water and A_{c} the PVT collector aperture area.

In Eq. (34), the overall heat-loss coefficient, U_{L}, can be estimated by,

$$U_{\text{L}} = U_{\text{top}} + U_{\text{back}}\,, \quad (36)$$

$$U_{\text{top}} = \frac{1}{\frac{1}{h_{\text{cv,g1a}} + h_{\text{rd,g1sky}}} + \frac{1}{h_{\text{cd,g1}}} + \frac{1}{h_{\text{cv,g1ig2}} + h_{\text{rd,g1ig2}} + h_{\text{rd,PVsky}}} + \frac{1}{h_{\text{cd,g2}}}}. \quad (37)$$

To express the useful heat in terms of the fluid inlet temperature, T_{in}, the heat removal factor, F_{R}, should be used, which represents the ratio of the actual useful energy gain that would result if the collector-absorbing surface had been at the local fluid temperature [86],

$$q_{\text{u}} = F_{\text{R}}\big(S - U_{\text{L}}(T_{\text{in}} - T_{\text{a}})\big)\,, \quad (38)$$

where,

$$F_{\mathrm{R}} = \frac{\dot{m}_{\mathrm{c}} c_{\mathrm{p}}}{A_{\mathrm{c}} U_{\mathrm{L}}} \left[1 - e^{\frac{-F' A_{\mathrm{c}} U_{\mathrm{L}}}{\dot{m}_{\mathrm{c}} c_{\mathrm{p}}}} \right], \tag{39}$$

$$F' = \frac{\frac{1}{U_{\mathrm{L}}}}{W \left[\frac{1}{U_{\mathrm{L}}(D + (W - D)F)} + \frac{1}{C_{\mathrm{bond}}} + \frac{1}{\pi D_{\mathrm{i}} h_{\mathrm{fi}}} \right]}, \tag{40}$$

$$F = \frac{\tanh\left[m \, \frac{W - D}{2} \right]}{\left[m \, \frac{W - D}{2} \right]}, \tag{41}$$

$$m = \sqrt{\frac{U_{\mathrm{L}}}{k_{\mathrm{abs}} \delta_{\mathrm{abs}} + k_{\mathrm{PV}} \delta_{\mathrm{PV}} + k_{\mathrm{eva}} \delta_{\mathrm{eva}}}}. \tag{42}$$

For the flat-box configuration (rectangular channels), the standard fin efficiency (F) and the collector fin efficiency factor (F') are simplified as follows,

$$F' = \frac{1}{1 + \frac{(W_{\mathrm{b}} + \delta_{\mathrm{abs}}) U_{\mathrm{L}}}{\pi D_{\mathrm{h}} h_{\mathrm{fi}}}}, \tag{43}$$

$$F = \frac{\tanh\left[\frac{m \, \delta_{\mathrm{abs}}}{2} \right]}{\frac{m \, \delta_{\mathrm{abs}}}{2}} = 1 . \tag{44}$$

In order to evaluate the convective heat transfer coefficient inside the collector channels (h_{fi}), the nature of the flow condition must be established by considering the Reynolds number, $Re = \rho_{\mathrm{w}} v_{\mathrm{w}} D_{i/\mathrm{h}} / \mu_{\mathrm{w}} = 4\dot{m}_{\mathrm{tube}} / (\pi D \mu_{\mathrm{w}})$, where $\dot{m}_{\mathrm{tube}}$ is the mass flow-rate of water flowing through each one of the riser tubes of the collector, μ_{w} is the dynamic viscosity of water, and $D_{i/\mathrm{h}}$ is the diameter of the riser tubes or the hydraulic diameter of the rise channel in the case of the flat-box configuration that has rectangular channels, where as $D_{\mathrm{h}} = 4A_{\mathrm{p}}/p$ [65]. In the present investigation, we have confirmed that the condition $Re < 3{,}000$ is always met, such that the flow is always laminar. For laminar flow, and assuming fully developed conditions, the Nusselt number is constant and the appropriate heat transfer coefficient correlation is $Nu = h_{\mathrm{fi}} D_{\mathrm{i/h}} / k_w = 4.36$ [3,6,89], with k_{w} the thermal conductivity of water.

The absorber plate temperature, T_{abs}, can be found by solving Eqs. (34) and (38) simultaneously, which gives,

$$T_{\mathrm{abs}} = T_{\mathrm{in}} + \frac{q_{\mathrm{u}}}{F_{\mathrm{R}} U_{\mathrm{L}}} (1 - F_{\mathrm{R}}) . \tag{45}$$

Rearranging equations, the mean fluid temperature, T_{fm}, can be estimated as [7],

$$T_{\mathrm{fm}} = T_{\mathrm{in}} + \frac{q_{\mathrm{u}}}{F_{\mathrm{R}} U_{\mathrm{L}}} \left(1 - \frac{F_{\mathrm{R}}}{F'} \right) . \tag{46}$$

Finally, according to the ASHRAE method, the thermal efficiency can be calculated from [7,15,86,94],

$$\eta_{\mathrm{th}} = \frac{q_{\mathrm{u}}}{I_{\mathrm{t}}} = F_{\mathrm{R}} (\tau\alpha)_{\mathrm{PV}} - F_{\mathrm{R}} U_{\mathrm{L}} \frac{T_{\mathrm{in}} - T_{\mathrm{a}}}{I_{\mathrm{t}}} . \tag{47}$$